ABSTRACT

Title of Thesis: MODELING AND ANALYSIS OF AN ACTIVE MAGNETORHEOLOGICAL SEAT AND LANDING GEAR SYSTEM TO PROTECT AN OCCUPANT IN A HELICOPTER CRASH

Caitlin Evelyne King
Master of Science, 2018

Thesis directed by: Professor Norman M. Wereley
Department of Aerospace Engineering

Occupant injuries in helicopter crashes occur primarily due to vertical loads. Mitigating those loads to the occupant is the best way to limit injuries sustained in an impact. Using magnetorheological dampers in the seat and landing gear can help to maximize the energy absorbed by the helicopter and minimize the loads to the occupant in a crash. There are a number of key interactions between the occupant models and the landing gear that have been examined in this research. These interactions are investigated and the control algorithms have been designed to reduce the loads transmitted to the occupant throughout the impact.

MODELING AND ANALYSIS OF AN ACTIVE MAGNETORHEOLOGICAL SEAT AND LANDING GEAR SYSTEM TO PROTECT AN OCCUPANT IN A HELICOPTER CRASH

by

Caitlin Evelyne King

Thesis submitted to the Faculty of the Graduate School of the
University of Maryland, College Park in partial fulfillment
of the requirements for the degree of
Master of Science
2018

Advisory Committee:
Professor Norman M. Wereley, Chair
Professor Sung Lee
Professor Brian Phillips

Acknowledgements

I want to firstly thank my advisor, Dr. Wereley, for his constant encouragement and guidance through this process. This has been a very valuable experience for me and I'm so thankful that he had a place for me in his lab.

I additionally want to thank my family for all their support. I've loved all of your messages and updates when I'm away and I am so glad I have a place to land whenever I get to come home.

I also want to thank the families and roommates who have adopted me along the way. Especially the Pedersens who opened up their home to me and provided me with a good meal and a bed whenever I needed it.

I'm very thankful to my lab mates for making this journey a fun one and helping me with all the steps along the way. Especially Jon, who listened and did his best to answer every question I asked.

I also want to thank my two best friends, Nathan and Keiko, who have called, emailed, or texted me every week while I've been in Maryland. Even though I live so far away from both of you, our friendships have remained as strong as ever.

Table of Contents

List of Tables

List of Figures

Nomenclature

a	acceleration
$a_{seatLimit}$	Limit of seat acceleration
C	Damping constant
C_c	Cushion damping constant
C_f	Correction factor
C_{total}	Total damping constant
$C_{suspension}$	Damping constant of suspension system
d	Stroke length
$d_{seatpan}$	Stroke length of seat pan
η	Efficiency
η_{seat}	Seat efficiency
$F_{95MaleLimit}$	Maximum force of 95th percentile male
$F_{MR_{seat}}$	MR force in seat
$F_{C_{seat}}$	Viscous force in seat
F_C	Damping force
$F_{C_{landinggear}}$	Viscous force in landing gear
F_d	Damper force
F_{MR}	Magnetorheological force
F_{yield}	Yield force (or MR force)
f_y	Yield force (or MR force)
F_K	Force from spring
g	Gravitational acceleration
G	Deceleration
G_{peak}	Deceleration peak
K	Stiffness constant
K_c	Cushion spring stiffness
K_{total}	Total spring stiffness
L_L	Limiting load
$L_{L_{peak}}$	Peak limiting load
M	Mass
M_{bio}	Biodynamic mass

$M_{occupant}$	Mass of occupant and seat
T	Time
t	Time
t_o	Initial time
v_o	Initial sink rate
$v_{seatpan}$	Velocity of seat pan
W_{seat}	Weight of seat
$W_{Eff95Male}$	Effective weight of 95th percentile male
$W_{clothes}$	Weight of clothes
W_{gear}	Weight of gear
y	Displacement
$\dot{y}$	Velocity
$\ddot{y}$	Acceleration
z	Displacement
$\dot{z}$	Velocity
$\ddot{z}$	Acceleration

List of Abbreviations

5F	5th percentile female
50M	50th percentile male
95M	95th percentile male
AMAD	Advanced Materials and Devices
BPM	Bingham plastic model
CFD	Computational fluid dynamics
COM	Compliant occupant model
CREEP	Container, Restraint, Energy absorption, Environment (local), Post crash factors
DRI	Dynamic Response Index
FLEA	Fixed load energy absorber
FMVSS	Federal Motor Vehicle Safety Standard
MR	Magnetorheological
ROM	Rigid occupant model
SBIR	Small business innovation research

Chapter 1: Introduction

The purpose of this chapter is to state the motivation for this research and set up the background information needed for full understanding of the project. This background knowledge includes helicopter crash dangers and protection system limitations, the injury criteria by which injuries are measured, and an introduction and summary of magnetorheological damper characteristics and behavior.

1.1 Motivation and Objectives

In the event of a helicopter crash, the occupant is placed in an extreme amount of risk for injury or death. Identifying, assessing, and limiting these risks are key steps that can greatly improve survivability and decrease the chance of injury. This research focuses on lowering the impact forces to the occupant by using an active crash protection system consisting of both a semi-active seat and a semi active landing gear. Models for the occupant, seat, and landing gear have all been placed together in tandem to determine how effective each system will be at lowering these loads. The objectives of this research are as follows:

- Create a comprehensive model of an occupant in a helicopter crash, including the occupant, seat, and landing gear

- Sequence the landing gear and seat crushing to absorb the maximum possible amount of energy
- Analyze the effect of occupant weight, sink rate, and load-stroke profiles on occupant survivability
- Investigate dynamic behavior of the models during an impact
- Determine the injury criteria most applicable to vertical impact loading

Additionally, some of the design specifications for the research are listed below:

- Sink rate: 12-42 ft/s (3.7-12.8 m/s)
- Seat stroke length: 16 $inches$ (40.8 cm)
- Landing gear stroke length: 3.25 $inches$ (8.25 cm)
- Occupant population size: 5th percentile female, 50th percentile male, 95th percentile male
- Helicopter: MD-500C

1.2 Helicopter Crash

Crashworthiness has been heavily researched over the past few decades [8]. As aircraft began flying faster, higher, and more frequently, crashes have become increasingly dangerous. Technologies have since been developed to help mitigate the hazards that arise during an impact. There are several types of these hazards

that have been categorized using the acronym "CREEP": Container, Restraint, Energy absorption, Environment (local), and Post crash factors [9]. "Container" focuses on avoiding structural collapse of the cabin and protecting from outside penetration into the occupied space. "Restraint" considers both restraining the occupant to their seats through harnesses or seat belts and restraining the seat to the aircraft so it does not rip out during the impact. This is one of the most influential aspects of crashworthiness design as it allows the occupant to receive the full benefits of the other crashworthy systems in place. "Energy absorption" refers to the systems in place that are designed to absorb the impact energy before it reaches the occupant. This area is the focus of this paper and will be discussed in depth. "Local environment" includes limiting the hazards within the occupant strike zone. Finally, "Post crash factors" refer to accounting for external hazards, such as fire, smoke, or water.

While all of these systems work together to decrease the potential for injury, occupants in helicopter crashes are typically injured in three basic ways: acceleration, contact, and environmental. Injuries from acceleration are caused from the general acceleration felt across the entire body in an impact. This can largely be mitigated by the energy absorption methods. Contact injuries are considered to be more localized and typically occur from the part of the occupant's body coming in contact with a part of the helicopter during the crash. These are typically dealt with in "Container", "Restraint", and "Environment". Environment, again, is the surroundings during and after the crash. This research focuses on the acceleration injuries.

As helicopters are typically lighter and smaller than most airplanes, space for crashworthy features is limited. The three main places these systems can be integrated are the seat, the floor, and the landing gear. These systems can be used to collapse strategically during the impact to absorb as much of the energy as possible. These effects can be seen in Fig. 1.1. A typical design requirement states that the loads should be mitigated up to impacts of 12.8 m/s without major injury [10]. This has already been achieved for the Black Hawk and Apache, and for these systems, fatalities are rare even at 15.2 m/s [11]. In smaller helicopters, though, it is difficult to reach this velocity safely.

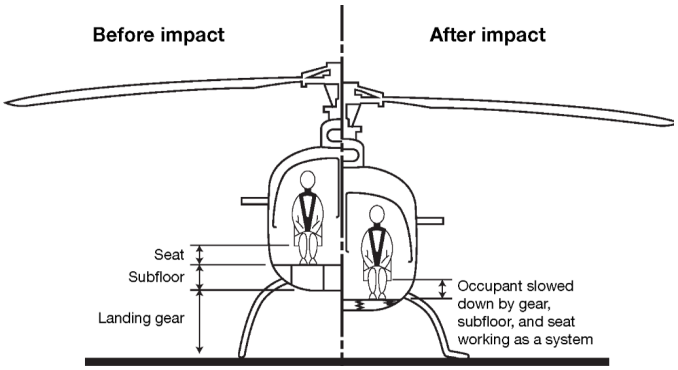

Figure 1.1: Diagram of helicopter energy absorbing components before and after the impact [1]

1.3 Injury Criteria

Humans have a long history of undergoing a wide range of impacts with varied results. While some low velocity impacts have caused serious injuries or even death, other high velocity impacts have been survivable [12]. Human tolerances to

these impacts have been studied and recorded for decades [13], [3].

Modeling and assessing the accelerations is a key step in designing systems to help protect occupants in real helicopter crashes. The models used in this project are discussed in Chapter 2. However, these models are not the only things needed to determine injuries. Once the simulations have been run, the accelerations and forces must be compared to injury criteria to determine whether or not the occupant was injured. In the past, there have been a large number of injury criteria that have been proposed, but there are few that have been designed and validated specifically for vertical impacts. Most tests have been performed on automobile impacts due to the higher demand and higher rate of accidents. Unfortunately, those are usually tested for frontal impacts and therefore do not apply well to the vertical loads seen in helicopter crashes. However, there are a few criteria that do apply to vertical impacts.

A long-held industry standard states that if the seat exceeds $14.5g$, the occupant will have a 20% chance of injury [2]. This, then, has become the target threshold in most design requirements. This standard originates from the $23g$ occupant limit for vertical impacts set in place by Eiband in 1959 [3]. Since occupant accelerations are not directly controllable like the seat pan is, Desjardins and Harrison calculated that the seat pan should experience a maximum of $14.5g$ so that the occupant is limited to $23g$. Their process of reaching that $14.5g$ threshold is summarized below.

4650 pounds is the highest force that the 95th% male can experience without exceeding $23g$ [2]. That force is then divided by the combined mass of the seat and

occupant, as shown in Eq. 1.1.

$$a_{seatLimit} = \frac{F_{95MaleLimit}}{W_{seat} + W_{Eff95Male}} = 14.62g \tag{1.1}$$

where:

$$W_{Eff95Male} = 0.8W_{95Male} + W_{clothes} + W_{gear} \tag{1.2}$$

The seat in their particular test weighed 152 *lbs* and the effective weight of the occupant came to 166 *lbs*. The missing 20% of the occupant's weight is likely the lower legs and feet, since those are supported by the floor and not the seat pan. Dividing the limiting load by these combined weights gives an acceleration limit of $14.62g$. Theoretically, if the seat is limited to a force that only accelerates the seat and occupant at $14.62g$, then that same force will accelerate the occupant alone at $23g$. Through a little more analysis, Desjardin and Harrison determined that the acceleration limit needs to be slightly less. As shown in Fig. 1.2 and Eq. 1.4, the seat pan deceleration efficiency was calculated and determined to be 0.62. By dividing the $14.62g$ acceleration limit by the seat pan efficiency, the potential peak loads to the occupant would experience can be estimated. Eq. 1.4 shows that the estimated peak acceleration would be $23.6g$, which is above the $23g$ limit. Therefore, the acceleration limiting value was lowered to $14.5g$.

$$\eta = \frac{\frac{1}{T}\int_{t_o}^{t} G dt}{G_{peak}} = \frac{\frac{1}{T}\int_{t_o}^{t} L_L dt}{L_{Lpeak}} \tag{1.3}$$

$$\frac{14.62g}{\eta_{seat}} = 23.6g \tag{1.4}$$

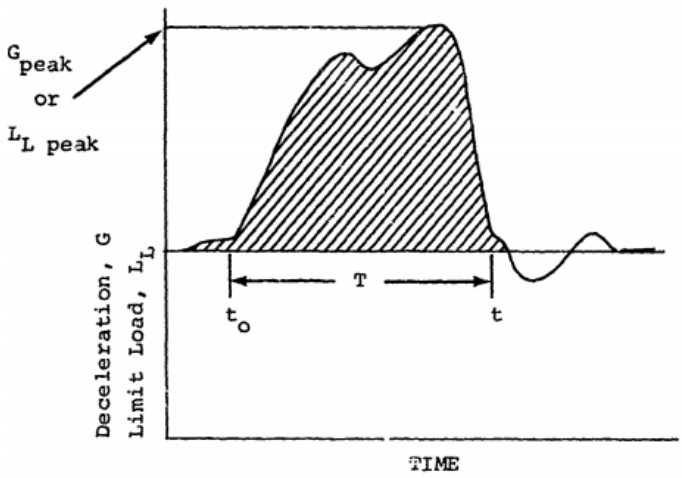

Figure 1.2: Deceleration of the seat used in Desjardin's and Harrison's calculations [2]

As shown in Eiband's tolerance curves in Fig. 1.3, voluntary, uninjured, undebilitated accelerations extend up to $14g$. Above this there is a region labeled "moderate injury," and above that starting at $42g$ is a region labeled "severe injury." One can reasonably assume that there is an unspecified region immediately above the $14g$ threshold where mild injury occurs. When this paper was written in 1959, ejection seats were accelerating their occupants at $23g$ without frequent or severe injury. Therefore, $23g$ was accepted as the upper tolerance for a human occupant experiencing upward acceleration. If the occupant experiences accelerations above $14g$, they will likely experience some form of injury, though it could be fairly mild. Once above $23g$, the severity of the injuries will likely increase to moderate or even severe levels depending on the pulse duration. Therefore, the $14.5g$ remains the target for seat accelerations during a vertical impact.

Several other injury criteria were also examined but were discarded for a

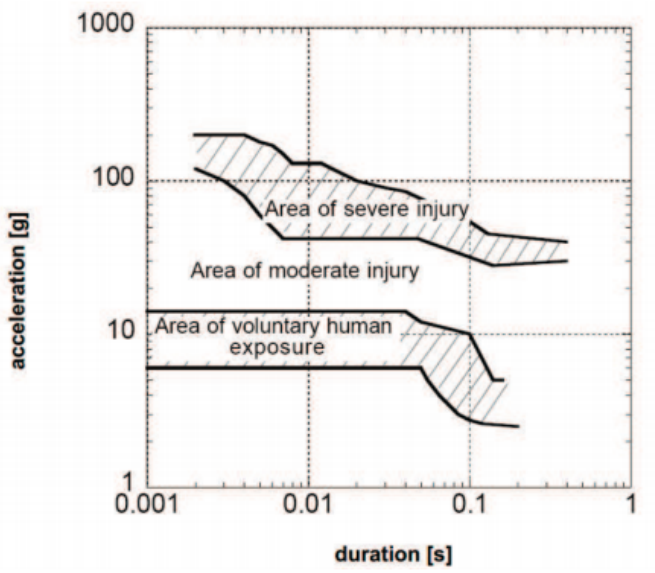

Figure 1.3: Acceleration human tolerance curves [3]

variety of reasons. The Dynamic Response Index (DRI) was investigated as it is a military injury criterion designed for determining damage to the lumbar portion of the spine from spinal compression in impacts [14], [15]. Unfortunately, this criterion had to be excluded because it is designed for impacts resulting in over $100g$. Most of the impacts this research looked at peaked at $50g$ at their worst before any energy absorbing devices were included to mitigate the loads.

Several automotive injury criteria were considered as well. Federal Motor Vehicle Safety Standard (FMVSS) 208 offers specific force limitations for each component of the body [16]. These forces have been expanded upon by Wereley and Choi [17], but they were excluded from this research because they are designed primarily for frontal loading instead of vertical loading.

1.4 Magnetorheological Damper Behavior

In order to achieve an active energy absorbing system, a magnetorheological (MR) damper model was used. Dampers have long been used as energy absorbing devices, but typical viscous dampers are passive and cannot accommodate multiple impact conditions. MR dampers, as shown in Fig. 1.4, work just like viscous dampers by pushing a fluid through an orifice in the piston head to resist the motion of the piston rod. The viscosity of the fluid and the size of the orifice have a direct effect on the damper's force output.

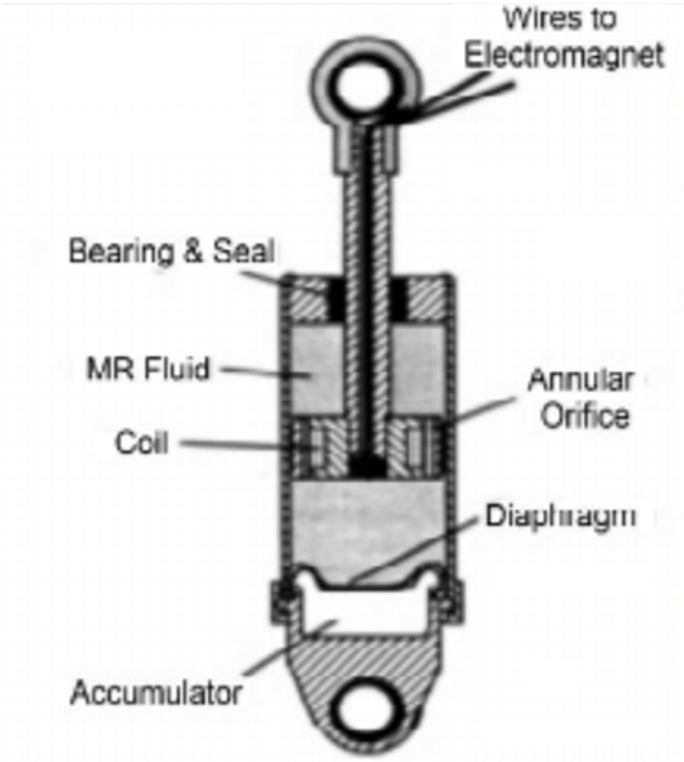

Figure 1.4: Typical viscous damper

MR dampers follow bingham plastic behavior, as seen in Fig. 1.5, but they have an adjustable yield stress because they use MR fluid instead of typical damper

fluids, like oil, water, or air. Magnetorheological fluid is a solution of microscopic magnetic particles (0.3-10 micron diameter) suspended in a hydrocarbon based carrier fluid [18]. These carbonyl iron particles form chains in the presence of a magnetic field, which increases the viscosity of the fluid and creates a yield stress, as shown in Fig. 1.5. As the magnetic field increases, so does the viscosity of the fluid. Therefore, the magnetic field can be varied to any value in order to control the yield force. This allows the damper's output force to reach a much wider range of forces and not be solely dependent on the piston velocity. When the magnetic field is turned off, the damper acts as a normal passive damper; the fluid flows through an open orifice, resisting the motion as the piston moves through the cylinder.

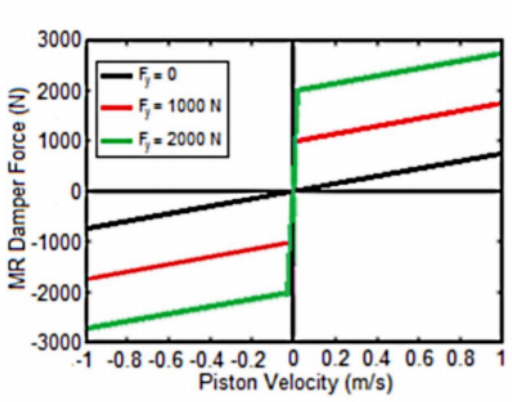

Figure 1.5: Bingham plastic model [4]

There is a short time delay between the change in current and the fluid's behavior change. This delay can be up to 10 ms, and for some MR applications, this must be considered. For helicopter crashes, however, this delay can be ignored. The most crucial moments of the crash are the first dozen or so milliseconds, and the MR damper can be tuned to the needed value based on the other sensors on the

helicopter having alerted the damper to the imminent crash.

This semi-active system allows for greater force controllability than a passive system without the complexity or weight of a fully active system. This versatile system is ideal for helicopter crash load attenuation.

Chapter 2: Models

The purpose of this chapter is to introduce the models used in this research. This research pairs one occupant model with one landing gear model for simulated crashes, though there are multiple options within each of those categories. The rigid occupant model and the compliant occupant model are discussed in Sec. 2.1 and 2.2 respectively. The landing gear models are discussed in Sec. 2.3. Interactions within and between models of this helicopter are the core of this research. Fig. 1.1 helps to visualize how the helicopter collapses under the occupant in the event of a crash. Fig. 2.1 shows how the models interact with each other, using the rigid model as described in Sec. 2.1.

There are two occupant models examined in this paper: the rigid occupant model and the compliant occupant model. Both models are designed for vertical impacts and have the same seat suspension system parameters. The rigid model is a simplified system while the compliant occupant model allows the analysis to look at individual components to offer a more complete picture of the accelerations and interactions within the occupant. Both occupant models have three different sizes: 5^{th} percentile female, 50^{th} percentile male, and 95^{th} percentile male, whose total masses and designations can be seen in Table 2.1. These three masses correspond

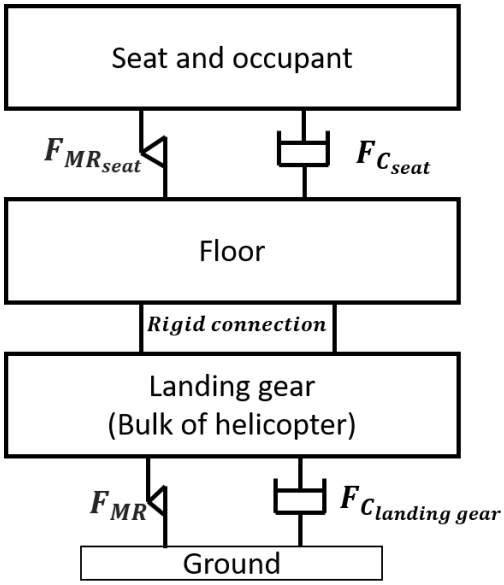

Figure 2.1: Helicopter and rigid occupant model

to the average and two extremes of the population that the crashworthiness system would be likely to see. The weight description is broken down and further explained in Sec. 2.2. It is worth noting, though, that these masses are likely an underestimation of typical military pilots as certain components have been excluded and no additional gear or equipment is included in the overall mass.

Table 2.1: Occupant Masses and Designations

Size	Mass	Weight	Designation
5^{th} percentile Female	49 kg	108 lbs	5F
50^{th} percentile Male	72 kg	158 lbs	50M
95^{th} percentile Male	101 kg	223 lbs	95M

The landing gear model is described in Sec. 2.3. This landing gear is based on the MD-500C helicopter, seen in Fig. 2.2 in its test set up for a full drop test [5], and is used in this research to support the entire weight of the helicopter

and occupant. The floor is considered to be rigid and does not collapse during the impact. The landing gear skids spread apart as the helicopter crashes.

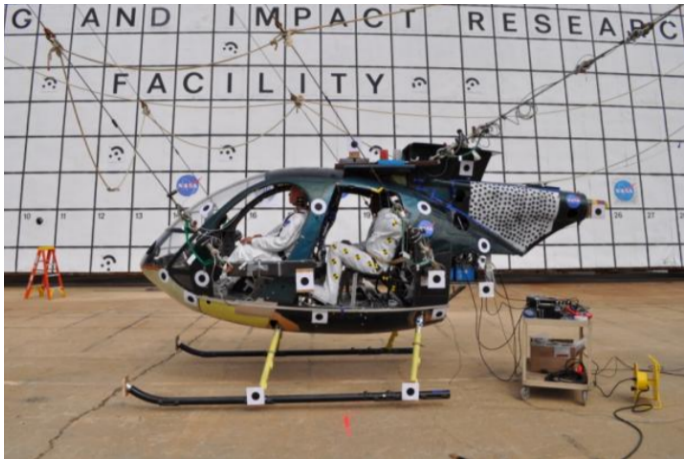

Figure 2.2: MD-500 helicopter test set up [5]

2.1 Rigid Occupant Model

Occupant models are an integral part of simulating helicopter crashes and determining if a new design will function as expected. There are many human occupant models that have been designed over the decades of crashworthiness research. The automotive industry has some very in depth, accurate models for many different types of collisions. However, most of those models are designed for frontal or lateral impacts. Very few car accidents, if any, send large vertical loads through the occupant like those that would be seen in a helicopter crash. Within vertically loaded models, there are two categories: vibratory models and impact models. In the event of a crash, human bodies stiffen significantly. This provides more support to the internal organs than in the relaxed body that the vibratory models are based

off, which severely changes their motion profile. This means that vertically loaded vibratory models are not a good representation of an occupant in a helicopter crash. The models are too soft and show much more motion than what happens in reality. Therefore, a different model must be used.

Often, a rigid occupant model is used instead of a compliant vibratory model. This model, as seen in Fig. 2.3(a), with its accompanying governing equation in Eq. 2.1, assumes that the entire occupant and seat are a single mass and that there are no dynamic interactions between the occupant and seat suspension system. This model is very simplistic and lacks the details and some of the accuracy afforded by the compliant occupant model. Springs are typically included in vibratory models as they are the sole method of returning energy to allow the seat to reach its original position before experiencing another vibratory cycle. However, springs are not desired in crash seats because they will cause the occupant to rebound, which forces the spine to go into tension. The human spine has a much lower injury threshold for tension than in compression and is therefore very undesirable. Sometimes a seat cushion is included in the model. This addition, seen in Fig. 2.3(b), adds a stiff spring.

$$M(\ddot{z} - \ddot{y}) + C(\dot{z} - \dot{y}) + f_{yield} = -Mg \tag{2.1}$$

where M, C, and K are the mass, damping constant, and stiffness constant respectively and g is the acceleration of gravity.

The cushion's mass is not included because it is so small when compared

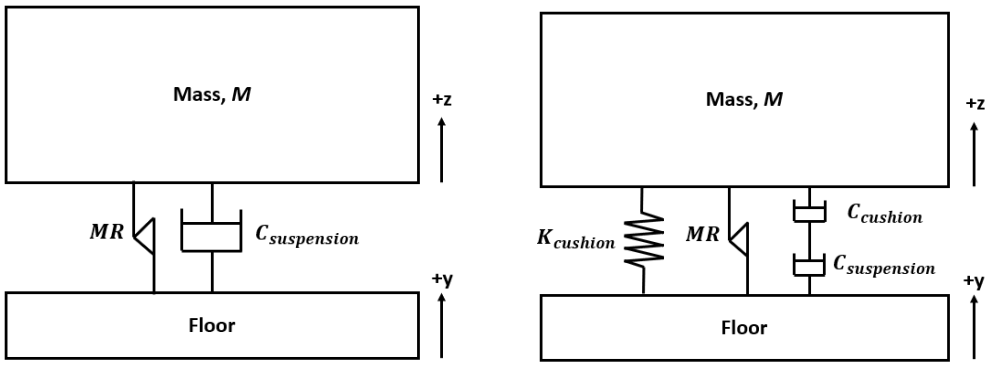

(a) Without cushion (b) With cushion

Figure 2.3: Rigid occupant model with and without cushion

to the rest of the system. Additionally, the cushion mass exhibits high frequency motion, which has very little effect on the low frequency motions on which these injury criteria are focusing. Therefore, the cushion mass is overlooked in favor of simplicity. The cushion parameters are C = 159 Ns/m and K = 37.7 kN/m [19].

$$M(\ddot{z} - \ddot{y}) + C_{total}(\dot{z} - \dot{y}) + f_{yield} + K(z - y) = -Mg \tag{2.2}$$

where C_{total} is found in Eq. 2.3.

$$C_{total} = \frac{C_c C_s}{C_c + C_s} \tag{2.3}$$

This cushion model was included in a few early simulations but was eventually excluded for simplicity. However, it was again included in the simulations performed in Ch. 6.

2.2 Compliant Occupant Model

The compliant occupant model is a more complete solution as it includes the responses from the seat pan, pelvis, viscera, chest, and head. While there are many vibratory models that have been developed [20], [21], [22], none of them apply well to impacts as they are all too soft to accurately model the forces within the occupant. Therefore, a multi degree of freedom model was developed by Singh and Wereley [23] and validated against the Sikorsky Advanced Composite Airframe Program (ACAP) test crash data gathered by Jackson et al. [24]. The masses originally used for this model were obtained from the Hybrid II 50^{th} percentile Male Test Dummy [25] and have been updated to the Hybrid III 50^{th}percentile Male Test Dummy, both of whose values are shown below in Table 2.2. The Hybrid III 5^{th} percentile Female Test Dummy masses and the Hybrid III 95^{th} percentile Male Test Dummy masses are also shown, as analysis has been done on these occupant sizes as well. The seat pan mass was taken from Choi and Wereley [17].

Table 2.2: Test Dummy Component Masses

Occupant	Head, kg M_1	Chest, kg M_2	Viscera, kg M_3	Pelvis, kg M_4	Seat, kg M_5	Total, kg
Hybrid II 50^{th}% Male	5.08	33.7	1.40	16.69	13.5	70.37
Hybrid III 5^{th}% Female	4.65	24.31	1.00	6.27	13.5	49.73
Hybrid III 50^{th}% Male	6.08	38.83	1.40	12.0	13.5	71.83
Hybrid III 95^{th}% Male	6.62	50.57	2.00	16.42	13.5	89.1

The arms were excluded from these masses because they are not rigid or secured during impact and are difficult to model. The lower legs were excluded as

they are assumed to be supported by the floor and not the seat suspension system. Additionally, the viscera masses were taken out of the chest mass and corresponds to a single organ about the size of the liver. The Hybrid III Test Dummies have a higher proportion of their weight distributed in their chests than the Hybrid II Dummies. Most of the changes between the two models came from moving about 5 kg from the pelvis to the chest. The head also increased in mass, while the anthropomorphic test dummy's (ATD) lower legs, not included in this model, decreased. While this redistribution causes higher forces to be reported from the chest, the accelerations from each component experienced no significant changes when using the Hybrid III masses.

Singh's model was validated for the 50^{th} percentile male, but not the 5^{th} percentile female or the 95^{th} percentile male. This research has done some analysis on the 5^{th} percentile female and 95^{th} percentile male occupants by substituting the appropriate masses in for the chosen occupant and scaling the viscera mass to an approximate, reasonable size. An attempt was made to scale the spring stiffnesses and damping constants as well, but this became complicated by their nonlinear nature. As such, the springs and dampers were left at their original values and only the masses were changed when evaluating other sized occupants.

The compliant occupant model is shown below in Fig. 2.4, along with the governing equations in Eqs. 2.4-2.8.

$$M_1\ddot{z}_1 = -F_{K_{1,2}} - F_{C_{1,2}} \tag{2.4}$$

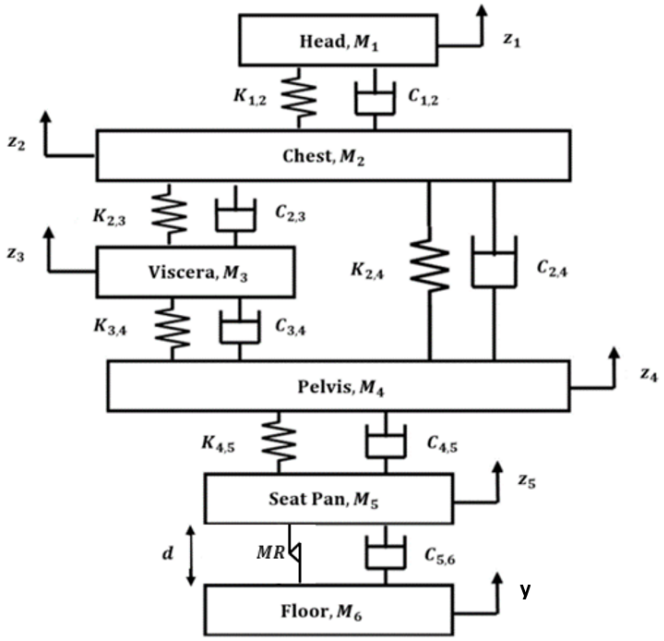

Figure 2.4: Compliant occupant model without cushion

$$M_2\ddot{z}_2 = F_{K_{1,2}} + F_{C_{1,2}} - F_{K_{2,3}} - F_{C_{2,3}} - F_{K_{2,4}} - F_{C_{2,4}} \tag{2.5}$$

$$M_3\ddot{z}_3 = F_{K_{2,3}} + F_{C_{2,3}} - F_{K_{3,4}} - F_{C_{3,4}} \tag{2.6}$$

$$M_4\ddot{z}_4 = F_{K_{3,4}} + F_{C_{3,4}} + F_{K_{2,4}} + F_{C_{2,4}} - F_{K_{4,5}} - F_{C_{4,5}} \tag{2.7}$$

$$M_5\ddot{z}_5 = F_{K_{4,5}} + F_{C_{4,5}} - F_{K_{5,6}} - F_{C_{5,6}} \tag{2.8}$$

$$F_{K_{i,j}} = K_{i,j}(z_i(t) - z_j(t)) \tag{2.9}$$

$$F_{C_{i,j}} = C_{i,j}(\dot{z}_i(t) - \dot{z}_j(t)) \tag{2.10}$$

where stiffness and damping coefficients are nonlinear values whose equations are shown below:

$$K_{i,j} = \alpha_{i,j} + \beta_{i,j}|z_i(t) - z_j(t)|^{\gamma_{i,j}} \tag{2.11}$$

$$C_{i,j} = \phi_{i,j} + \chi_{i,j}|\dot{z}_i(t) - \dot{z}_j(t)|^{\psi_{i,j}} \tag{2.12}$$

The spring and damper constants for these equations are shown in Table 2.3.

Table 2.3: Stiffness and Damping Constants

Biodynamic Parameter	$\alpha, N/m$		$\beta, N/m^{1+\gamma}$		γ		$\psi, N \cdot s/m$		$\chi, N \cdot s^{1+\psi}/m^{1+\psi}$		ψ	
Head-Chest	$\alpha_{1,2}$	$5.12e+6$	$\beta_{1,2}$	101	$\gamma_{1,2}$	1.658	$\phi_{1,2}$	102	$\chi_{1,2}$	103	$\psi_{1,2}$	5.592
Chest-Viscera	$\alpha_{2,3}$	$9.77e+6$	$\beta_{2,3}$	$1.47e+6$	$\gamma_{2,3}$	4.279	$\phi_{2,3}$	104	$\chi_{2,3}$	$1.23e+4$	$\psi_{2,3}$	1
Chest-Pelvis	$\alpha_{2,4}$	$2.45e+6$	$\beta_{2,4}$	$9.09e+6$	$\gamma_{2,4}$	0.489	$\phi_{2,4}$	3.76e+3	$\chi_{2,4}$	$6.99e+4$	$\psi_{2,4}$	1.195
Viscera-Pelvis	$\alpha_{3,4}$	$4.88e+6$	$\beta_{3,4}$	$5.56e+6$	$\gamma_{3,4}$	3.962	$\phi_{3,4}$	104	$\chi_{3,4}$	$1.51e+4$	$\psi_{3,4}$	1.145
Pelvis-Seat Pan	$\alpha_{4,5}$	105	$\beta_{3,4}$	$3.32e+6$	$\gamma_{3,4}$	0.816	$\phi_{3,4}$	110	$\chi_{3,4}$	112	$\psi_{3,4}$	2.034

This model, like the rigid model, can also include a seat cushion. The addition is shown below in Fig. 2.5. The only equations to change are Eq. 2.7 and Eq. 2.8, which become Eq. 2.13 and Eq. 2.14 respectively.

$$M_4\ddot{z}_4 = F_{K_{3,4}} + F_{C_{3,4}} + F_{K_{2,4}} + F_{C_{2,4}} - F_{K_{total,4,5}} - F_{C_{total,4,5}} \tag{2.13}$$

$$M_5\ddot{z}_5 = F_{K_{total,4,5}} + F_{C_{total,4,5}} - F_{K_{5,6}} - F_{C_{5,6}} \tag{2.14}$$

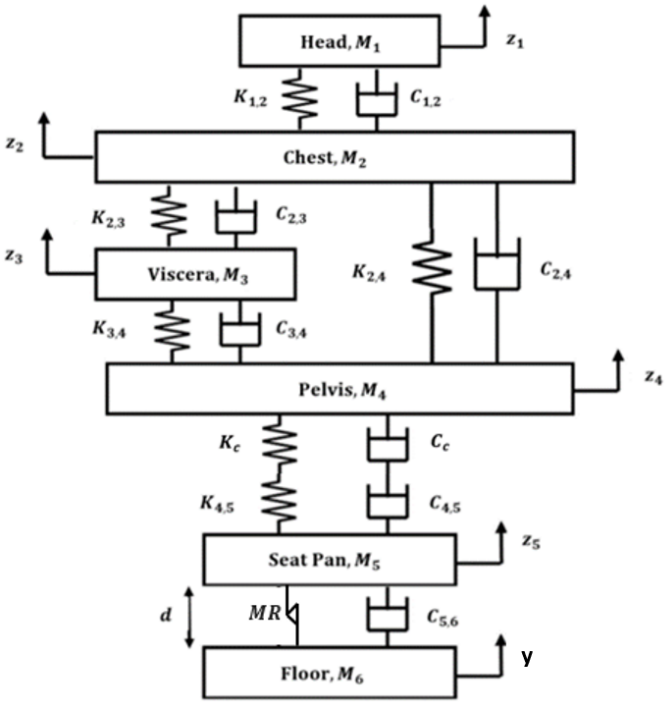

Figure 2.5: Compliant occupant model with cushion

$$C_{total,4,5} = \frac{C_{4,5}C_c}{C_{4,5} + C_c} \tag{2.15}$$

$$K_{total,4,5} = \frac{K_{4,5}K_c}{K_{4,5} + K_c} \tag{2.16}$$

Unfortunately, Singh's model is not perfect. While it does have more degrees of freedom and therefore more specificity than the rigid occupant model, this model has only been validated with the 50^{th} percentile male in a single helicopter test crash. Without additional testing, there is no way to know how far that validity extends in terms of occupant size or initial helicopter sink rate. This model is much too stiff to be used for low g impacts, as seen in vibratory tests, and no other sized occupants have been tested. Additionally, this model is not as simple as the rigid

model and is accompanied by the computational time burden typical with more complex systems.

2.3 Landing Gear Model

The landing gear on a helicopter is one of the primary locations that energy absorption equipment can be added. Helicopter crashes occur over a large sink rate range, with large payload variations, and across a wide variety of ground conditions [26]. All of these factors can have an impact on the effectiveness of the landing gear systems. A passive damping system is not capable of adapting to all of these different factors and a great deal of energy may be transmitted to the occupant rather than being absorbed by the systems in place. An active or semi-active landing gear can account for many of these conditions, adapt in real time to absorb a much larger amount of energy, and not transmit excess energy to the occupant.

A new, semi-active model was developed for the landing gear in a 2250 lb MD-500C helicopter, pictured in Fig. 2.2. The MD-500 helicopter is a lightweight helicopter that has been used in previous modeling and testing [27]. This model was originally created by Choi et al. in 2016 and it was designed to work over a sink rate range of 6-12 ft/s [6]. This theoretical landing gear outputs 4000 pounds of force for each of the four dampers on landing gear and strokes for 8.25 cm. As seen in Fig. 2.6, at low sink rates the combined MR and viscous forces are not high enough to reach the target force. The MR force is turned up to its maximum possible force, but the additional viscous force is still needed, and the target force

is not reached until a sink rate of 6 ft/s. At this point, the MR force is decreased as the viscous force increases in order to maintain the target net force. At 12 ft/s, the MR force is turned off completely and the damper force is completely viscous based. This design and its control algorithms were tested at low sink rates using ramp displacement inputs on a servo-hydraulic testing machine and at high speeds using single drop damper tests.

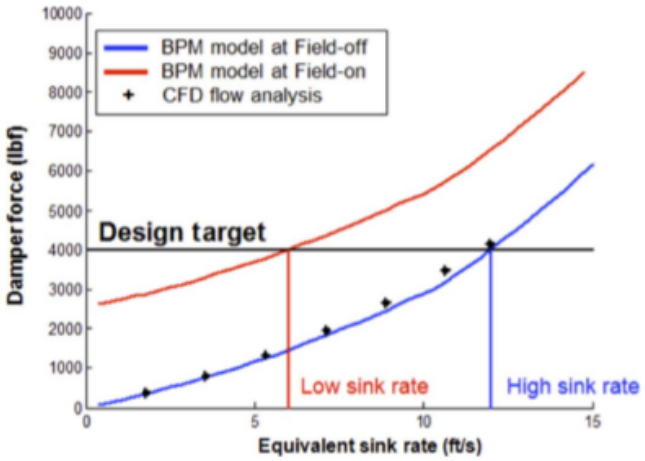

Figure 2.6: Passive and MR damper force components [6]

This work was then expanded upon by Powell et al. [7] when a passive relief valve was added to the damper to increase the effective sink rate maximum up to 26 ft/s. With the addition of the spring assisted passive relief valve, the relief valve opens when the sink rate reaches 12 ft/s, which lets more fluid through without increasing the output force. This allows the maximum sink rate to increase up to 26 ft/s before the seal cannot open any further and the damper force exceeds the target force. Powell's model's output, shown in Fig. 2.7, includes the force from the piston motion, the MR force, and the transition between the "On"and "Off" states

of the damper. This model is very complex and requires more computing time than the rest of the combined models. Therefore, several other simplified models have been proposed to be used in place of Powell's model for this research.

Three other simplified models were investigated, all seen in Fig. 2.8. The first is a constant stroking load model. This idealized model provides a constant force of 72 kN (4000 lbs from each of the four dampers) across the entire stroke. The second model is the hyperbolic tangent model, which is similar to the constant stroking load model, but includes a more realistic "ramp up" period. Finally, the third model is the sinusoidal model. This model most closely matches Powell's model without the additional computing time. Each of these models reaches the desired 72 kN, but with varying load stroke profiles. Since the constant stroking load landing gear is nearly 50% more efficient than the more realistic sinusoidal landing gear, seen in Fig. 2.9, it was used to determine the best-case scenario for the occupant in most of the simulations in Ch. 4 and Ch.5.

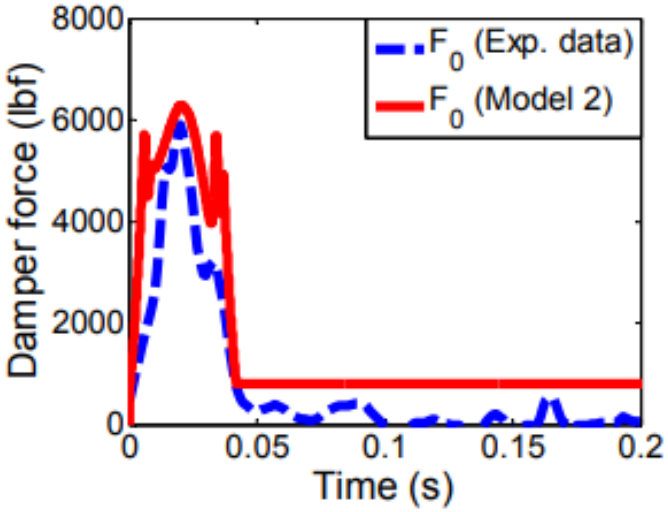

Figure 2.7: Powell's landing gear model [7]

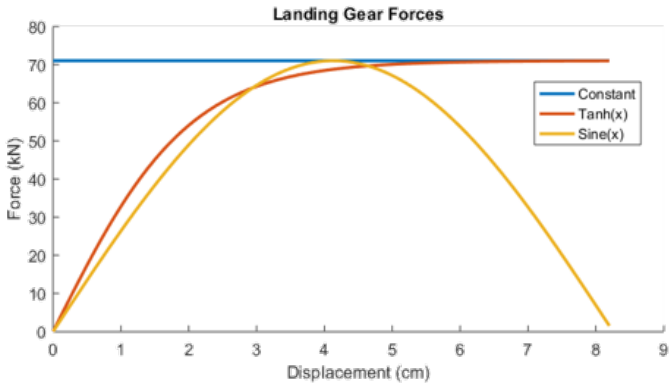

Figure 2.8: Three simple landing gear options

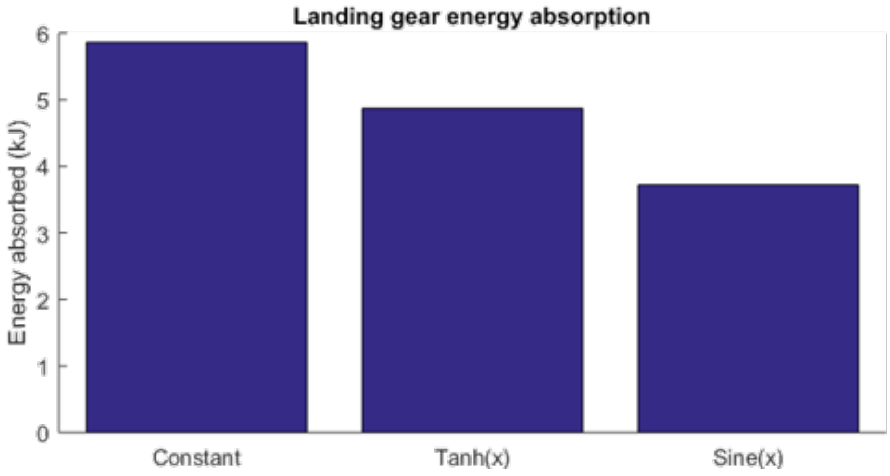

Figure 2.9: Energy absorbed by each landing gear model

Chapter 3: Seat Damper Forces

The purpose of this chapter is to investigate several different load-stroke profiles for the seat damper. These options include completely passive methods, like the viscous damper and fixed load damper, and semi-active methods, like the adjustable fixed load damper and variable load damper. These semi-active behaviors are achieved by introducing a magnetorheological damper into the seat's suspension system. This controllable damper can be adjusted to output the minimum necessary force throughout the impact to lower the loads to the occupant, as explained in Sec. 1.4.

Active seats are integral to improving helicopter crash survivability and increasing the maximum survivable impact velocity. Passive seats, while simple and well-studied, have a narrow range of maximum efficiency conditions, and their inefficiencies lead to a higher probability of injury for atypical occupants. That is, occupants above or below the designed weight are progressively more in danger during an impact. Previous seat energy absorbers have been passive and designed for a single mass and velocity combination.

3.1 Viscous Forces

Viscous energy absorbers are very simple devices and have long been used as energy absorbers in helicopter seats. These passive dampers were designed for the 50th percentile male (50M) at a specific impact velocity. Fig. 3.1 shows the effects of imperfect conditions. These following simulations use a 16 inch seat stroke length, no landing gear model, and the rigid occupant model. When the 50M impacts at 7.25 m/s, the system works at its maximum efficiency; the occupant uses exactly the entire stroke length and his peak loads are at his injury threshold. When the 50M impacts at lower velocities, however, he does not use the full stroke length. This wastes some of the energy absorption capabilities of the damper and therefore increases the peak loads on the occupant. Finally, if the sink rate is greater than 7.25 m/s, the 50M clearly exceeds his injury threshold and exhausts the stroke. Since the damper cannot dissipate enough energy before it bottoms out, a large stopping force is imparted to the occupant. This stopping force are extremely dangerous and can easily cause injuries. Impact velocities above 7.25 m/s require longer stroke lengths to absorb enough energy.

These inefficiencies also affect other occupant sizes. Fig. 3.2 shows three occupants each impacting at 7.25 m/s on a viscous system. The 50th percentile male uses the exact stroke length and his peak force does not exceed his injury threshold. The 5th percentile female, however, has a lower injury threshold due to her smaller mass. Her loads exceed her injury threshold and the damper stops her too early, wasting stroke length. Had the system been able to adapt to her smaller

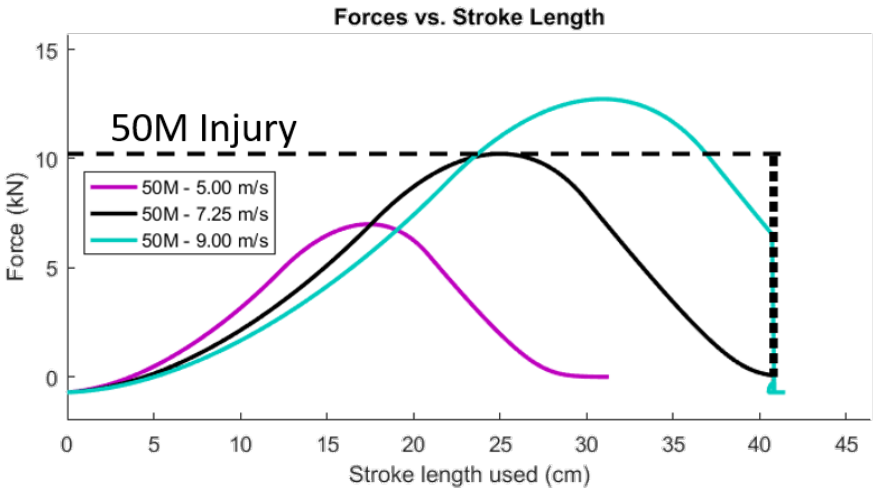

Figure 3.1: 50M impacting at three velocities on viscous damping system

mass, she could have used the full stroke length and potentially lowered her peak loads to below her injury threshold. Finally, the 95th percentile male is too heavy for the viscous system to handle at 7.25 m/s and he exhausts his stroke length. This means that he is very likely to be injured by the stopping force, even though he never reaches his injury threshold up until that point.

It is clear that the viscous damping system has many shortcomings. While it is simple, well tested, and lightweight, it also cannot adapt to multiple occupants or sink rates, and even at its most efficient, the viscous damper can absorb less than half of the available energy. To solve some of these problems, a fixed load energy absorber was designed and implemented, as described in Sec. 3.2.

3.2 Fixed Load Energy Absorber

The fixed load energy absorber (FLEA) is a device designed to supply a constant load to the seat throughout the crash [28]. This system is typically designed

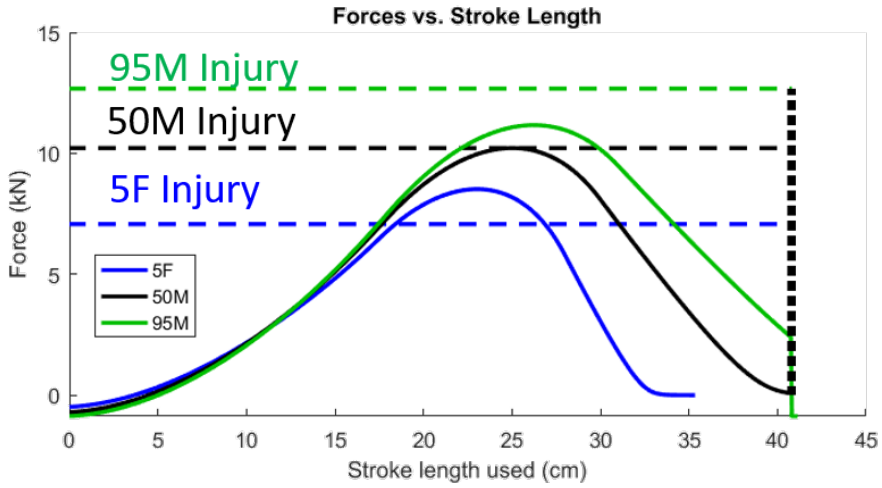

Figure 3.2: Three occupant masses impacting at 7.25 m/s using viscous damping system

to stroke at the 50th percentile male's injury threshold. This maximizes the energy absorption possible by providing the maximum force to the occupant across the entire stroke. This increased efficiency allows the maximum safe sink rate to increase from the viscous system's 7.25 m/s up to 10.7 m/s.

However, some of the fixed load energy absorber's shortcomings can be seen in Figs. 3.3 and 3.4. Fig. 3.3 shows the 50th percentile male at three different sink rates. The fixed load energy absorber works perfectly for the 10.7 m/s sink rate; this sink rate uses exactly the full stroke length and then brings the occupant to a gentle stop. However, this system exacerbates the problems the viscous system had at lower sink rates. Since the fixed load energy absorber strokes at a specific force, this means that it both wastes some of the stroke length and does not reduce any of the loads. Additionally, sink rates higher than 10.7 m/s will exceed the stroke length and the occupant will experience a dangerous stopping force.

Fig. 3.4 shows the larger problem with fixed load energy absorbers: they cannot adapt to different occupant masses. This figure shows all three rigid occupants impacting at 10.7 m/s. While the 50th percentile male experiences a soft landing and does not exceed his injury threshold, the 5th percentile female and 95th percentile male do not have such a smooth ride. The 5th percentile female wastes stroke length and exceeds her injury threshold by nearly 45%. The 95th percentile male never hits his injury threshold, but he exhausts his stroke if his sink rate is above 9.6 m/s.

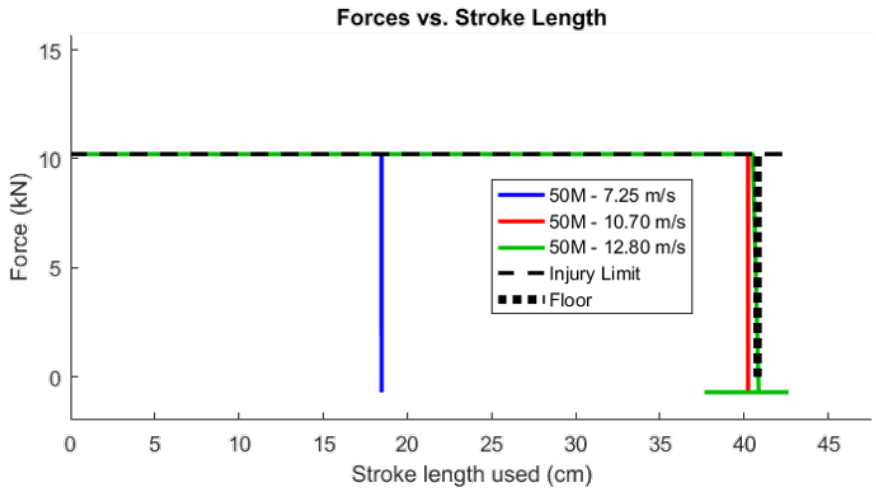

Figure 3.3: 50M at three speeds using fixed load system

These shortcomings and dangers can be mitigated at lower impact velocities by using an active system to absorb the energy.

3.3 Magnetorheological Damper

By incorporating an MR damper into the seat's energy absorber, the loads to the occupant can be greatly reduced. Fig. 3.5 shows the forces of a 50th percentile

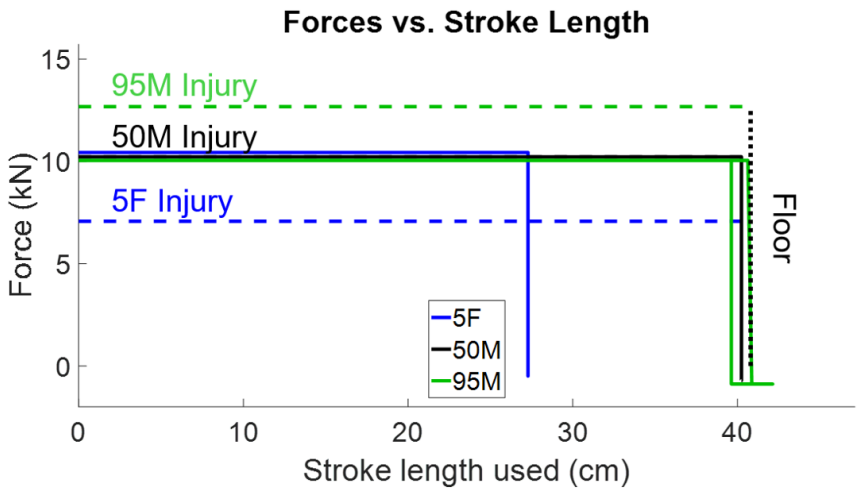

Figure 3.4: Three occupant masses using fixed load system at 10.7 m/s

male impacting at 7.25 m/s, which was the maximum safe sink rate of a purely viscous system. However, the added MR force combines with the viscous force to help create a net force much lower than the 50th percentile male's injury threshold. By setting the MR force to the maximum allowable force and having it vary inversely with the viscous force, the two can be added together to produce a constant net force much lower than the injury threshold across the entire stroke.

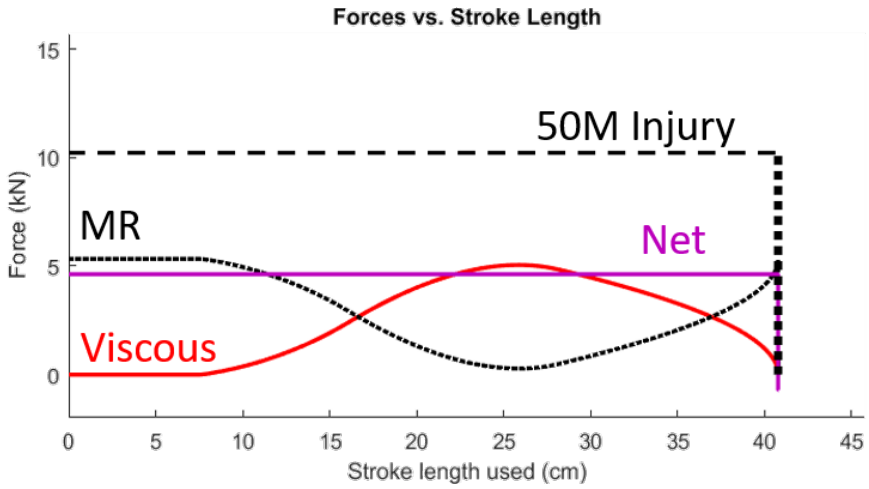

Figure 3.5: 50M using active MR system at 7.25 m/s

Since a semi-active system effectively transforms a viscous system into an adjustable fixed load system, the next logical step is applying it to all three occupants. While traditional fixed load energy absorbers are set to one output force, using an MR force can help to mitigate these limitations. Rather than having the viscous damping set to the 50th percentile male's threshold, the system should be designed such that the viscous damping does not exceed the 5th percentile female's injury threshold. Then, the MR force can be used to compensate for any additional needed force, which allows all three occupants experience a soft landing. This configuration with each occupant impacting at 10.7 m/s can be seen in Fig. 3.6.

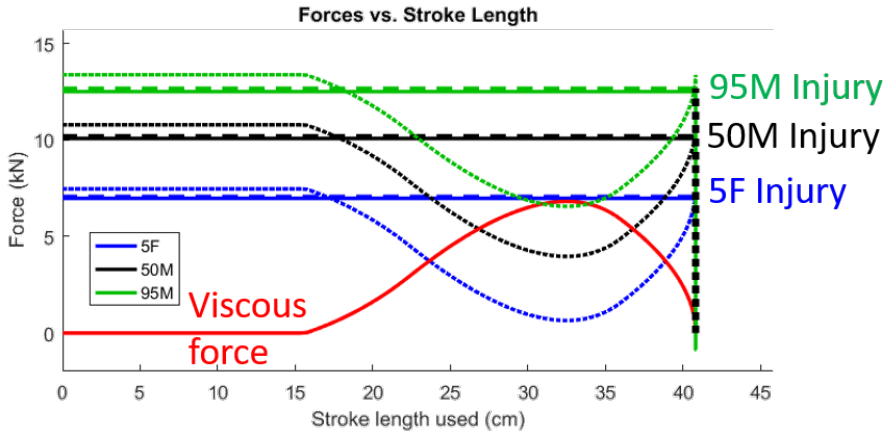

Figure 3.6: Three occupants using active MR system at 10.7 m/s

Using this method, all three occupants receive the lowest constant force necessary to bring them to a soft landing without wasting stroke length. 10.7 m/s is still the maximum impact velocity that a 16 inch stroke seat can handle, but the MR damper allows that threshold to be safely reached by all occupants.

The MR damper models used in this research are very idealized and are primarily being used as the model to determine the best-case scenario an occupant

can expect. A number of other, more realistic damper models have been developed and have been used to model and validate other experiments [29], [30].

3.4 Algorithm

The control algorithms for the occupant models are very similar to each other. Both are based off of the energy equation, shown in Eq. 3.1. The rigid occupant model's equations are shown in Eqs. 3.1-3.3 and the compliant occupant model's equation is shown in Eq. 3.4.

$$Mgd + \frac{Mv_o^2}{2} = F_d d \tag{3.1}$$

F_d can be solved for, seen in Eq. 3.2, to provide the necessary force to stop the seat pan at the end of the stroke length. From there, f_y can be calculated since the total damping force is just the sum of the viscous damping force and the yield force, shown in Eq. 3.3.

$$F_d = \frac{Mgd + \frac{Mv_o^2}{2}}{d} \tag{3.2}$$

$$f_y = F_d - C(\dot{z} - \dot{y}) \tag{3.3}$$

The compliant occupant model control algorithm is very similar to the rigid occupant model's control algorithm. Starting with Eq. 3.2, a few variables can be substituted in to accommodate the compliance of the new model.

$$F_d = \frac{M_{bio} g d_{seatpan} + \frac{M_{bio} v_{seatpan}^2}{2}}{d_{seatpan}} \tag{3.4}$$

where $M_{bio} = C_f M_{occupant}$ and C_f is a numerically determined correction factor designed to handle the internal dynamics of the compliant occupant model. The correction factor is discussed further in Sec. 3.4.1. Besides the correction factor, the major difference between the rigid occupant model control algorithm and the compliant occupant model control algorithm is that the COM control algorithm must be updated continuously throughout the crash while the ROM control algorithm is constant and can be set by the initial conditions of the crash.

Additional control methods have been developed by other researchers, though those algorithms are all much more complex than the ones used in this project [31], [32] .

3.4.1 Correction Factor

When the compliant model was first introduced, there was no mass correction factor. It was quickly discovered that the internal dynamics of the compliant occupant model affects the soft landing and induces a rebound after the landing. This rebound effect can be seen in Fig. 3.7.

To mitigate this dangerous outcome, many simulations were run and a numerically calculated correction factor was determined. This correction factor is a function of both occupant mass and initial sink rate and its equations can be seen in Eqs. 3.5-3.9.

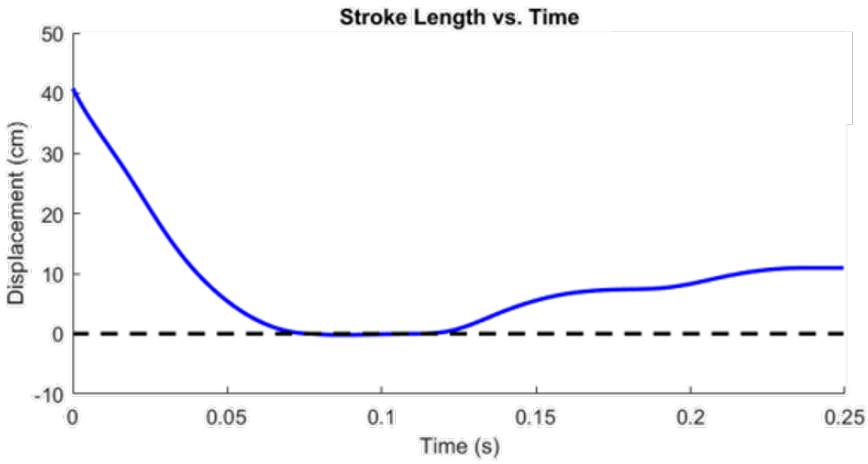

Figure 3.7: Rebound from compliant occupant without mass correction factor

$$C_f = Av_o^3 + Bv_o^2 + Cv_o + D \tag{3.5}$$

$$A = -4.4734 * 10^{-7}M^2 + 5.6731 * 10^{-5}M - .002 \tag{3.6}$$

$$B = -9.0973 * 10^{-6}M^2 + .0011M - .0442 \tag{3.7}$$

$$C = 5.3918 * 10^{-5}M^2 + .0062M - .3349 \tag{3.8}$$

$$D = -1.0230 * 10^{-4}M^2 + .0125M + .1548 \tag{3.9}$$

Fig. 3.8 shows how the necessary correction factor must increase in order to accommodate larger masses and sink rates. This correction factor effectively increases the amount of force the damper sends into the seat pan. The logical

question that follows is, "Why does increasing the upward force into the seat decrease the upward rebound?" Through the compliant occupant model simulations, it has been determined that most of the motion occurs between the pelvis and the seat pan. With the lower, unadjusted force, the seat pan is stopped in time, but the spring and damper between the seat pan and pelvis are soft enough to allow the pelvis to continue its descent. This spring eventually absorbs enough energy and releases it, pushing the occupant back up and pulling the seat pan with it. By increasing the force, this rebound effect can be dealt with during the descent in a much safer manner so that both the seat pan and the pelvis come to a stop at the end of the stroke length. There is still some rebound, seen in Fig. 3.9, but these only occur at very high sink rates and the effects have been lessened dramatically.

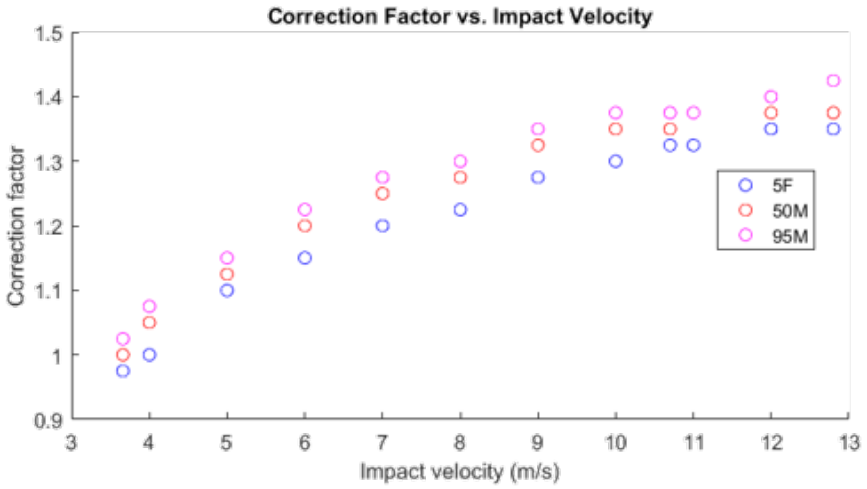

Figure 3.8: Mass correction factor necessary for soft landing for each occupant at each velocity

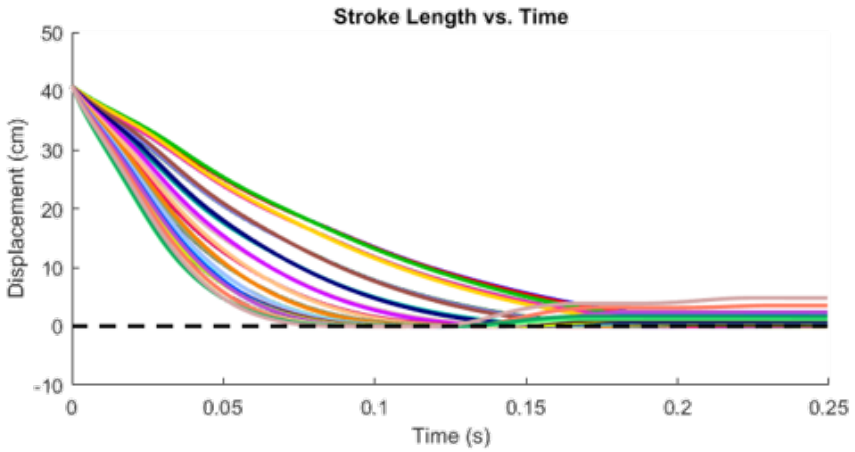

Figure 3.9: Stroke length with mass correction factor at multiple sink rates

Chapter 4: Rigid Occupant Model and Landing Gear

The purpose of this chapter is to examine the effects of the landing gear on the rigid occupant and determine the best device to limit the loads to the occupant. Since the rigid occupant model is such a simple case, the landing gear benefits are easily observed and the energy distribution is easy to track.

4.1 Results

The addition of the landing gear to the rigid occupant model produces some clear, beneficial results. The easiest way to gauge these benefits is to simulate the maximum safe sink rate from the seat alone, but including the landing gear model in the calculations as well. Fig. 4.1 shows the seat acceleration for the 50th percentile male impacting at 10.7 m/s. Energy is absorbed by the landing gear in the first 8 cm of the stroke. This absorbed energy means that the peak loads can be reduced across the rest of the seat's stroke once the landing gear has crushed completely. The constant stroking load landing gear reduces the peak accelerations on the occupant from 14.5g to 13.1g.

The more realistic, sinusoidal landing gear model was also examined to see its effect on the rigid occupant's accelerations. Since this model is only 60% as

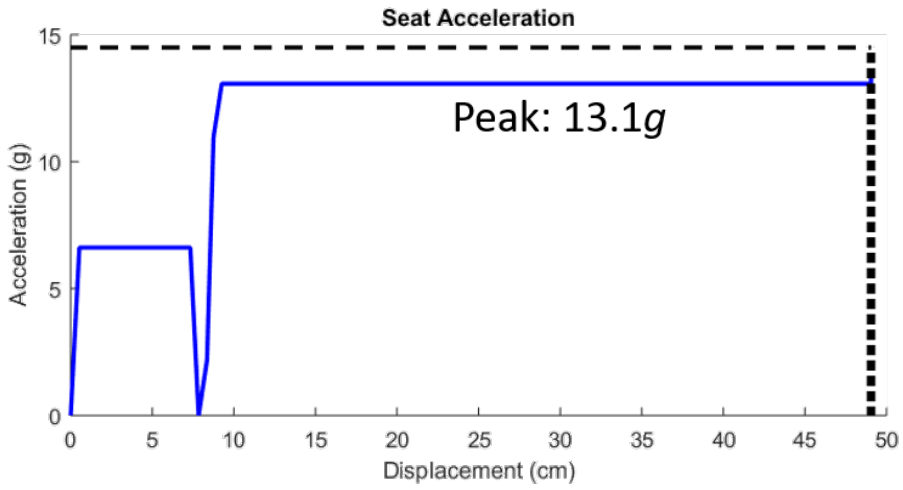

Figure 4.1: Rigid occupant model acceleration at 10.7 m/s with constant stroking load landing gear

efficient as the constant stroking load landing gear, the peak loads are not expected to drop as much. Fig. 4.2 shows that while the landing gear does still absorb some energy from the impact, it is nowhere near as effective and only drops the peak loads from 14.5g to 13.9g.

Once the landing gear was determined to benefit the seat throughout the impact in some manner, regardless of its load stroke profile, the sink rate was increased until the occupant was again peaking at 14.5g. This new sink rate was 11.2 m/s and the corresponding occupant accelerations are shown in Fig. 4.3.

While the landing gear certainly helps to increase the maximum safe sink rate, it also adds a very stiff element to the system that is detrimental to the occupant's safety at lower sink rates. The landing gear strokes at 6.7g regardless of whether the occupant would reach that threshold if the seat stroked freely across the entire stroke length. Fig. 4.4 shows the rigid occupant model impacting at various

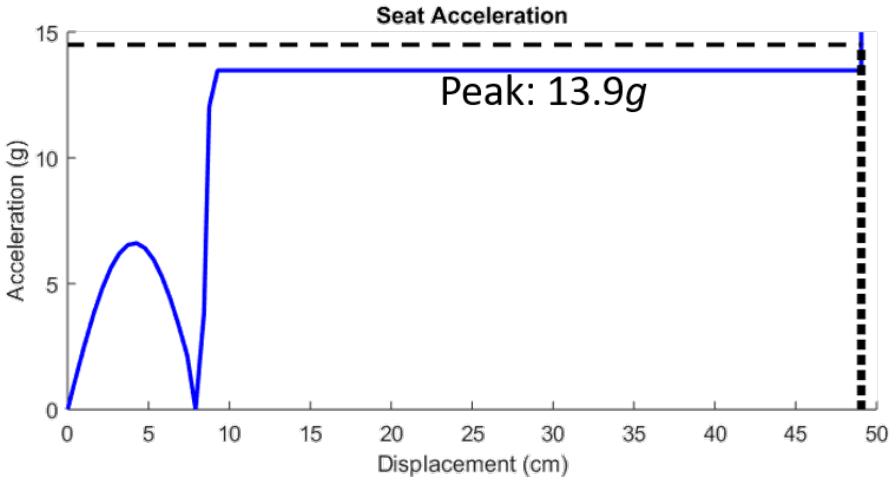

Figure 4.2: Rigid occupant model acceleration at 10.7 m/s with sinusoidal stroking load landing gear

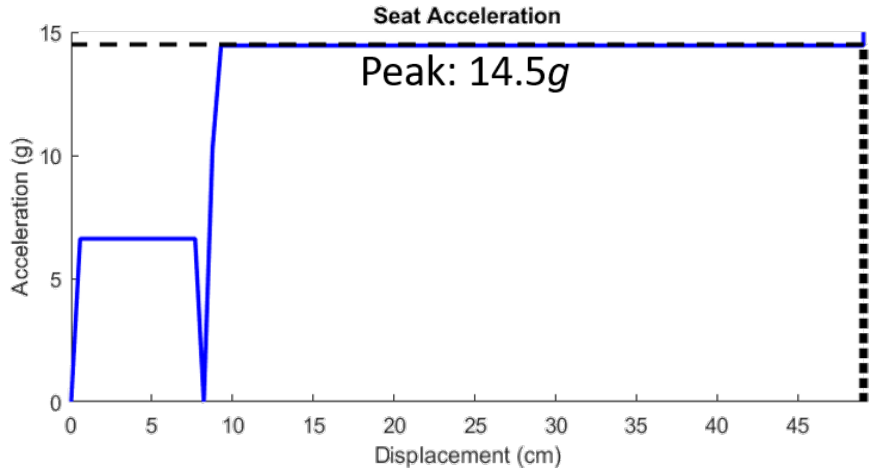

Figure 4.3: Rigid occupant model acceleration at 11.2 m/s with constant stroking load landing gear

sink rates and their accelerations after the landing gear crushes completely. Below 3.2 m/s, the landing gear absorbs all of the energy from the impact and the seat pan will not need to stroke. Interestingly, below 7.9 m/s, the seat will not stroke above the landing gear stroking threshold. This means that below 7.9 m/s, the landing gear is inducing higher loads on the occupant than would otherwise occur without the landing gear. Only above 7.9 m/s does the occupant start to experience higher loads from the seat crushing than they do from the landing gear.

This trade-off becomes a key issue when designing landing gear systems. The higher the landing gear's stroking threshold is, the more energy it will absorb and the more likely it will be able to protect the helicopter from damage. The higher the stroking load, though, the more likely the occupant will sustain some kind of injury, even if it is mild. This unadjustable stroking load also forces the system to behave more like the FLEA that the MR was added to avoid. While the landing gear only induces 6.7g on the rigid occupant, the compliant occupant interacts poorly with the landing gear at low sink rates. The compliant model's difficulties with the landing gear is discussed in Sec. 5.3.1.

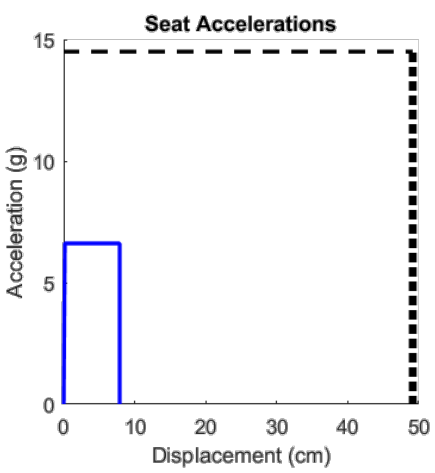

(a) 3.2 m/s

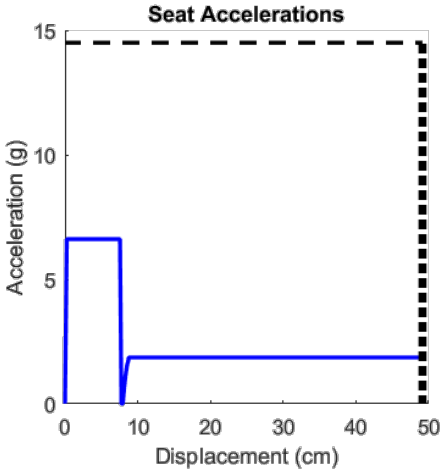

(b) 5 m/s

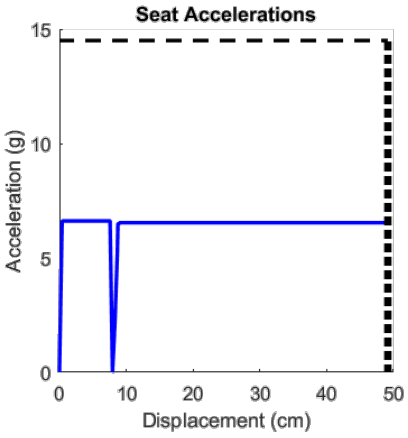

(c) 7.9 m/s

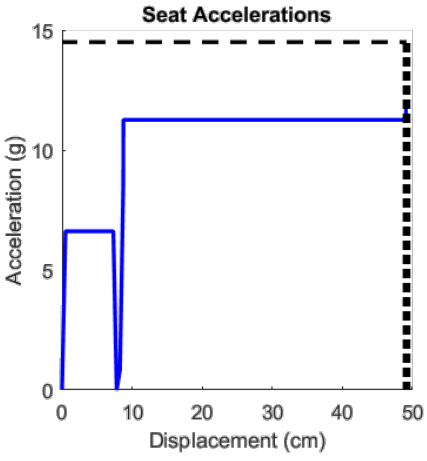

(d) 10 m/s

Figure 4.4: Rigid occupant model seat accelerations at various sink rates

Chapter 5: Compliant Occupant Model and Landing Gear

The purpose of this chapter is to examine how the landing gear and the compliant occupant model can work together to limit the loads to the occupant during a crash. The internal dynamics in the compliant model interact heavily with the seat pan and landing gear to produce some interesting results and add a number of complications.

5.1 Compliant Occupant Model Alone

Before looking at the compliant occupant model's interactions with the seat pan, the compliant occupant model must be examined on its own. While the rigid occupant model was very straight forward with few complications, the compliant model is much more complex. Sec. 5.1.1 looks at the development process of the control algorithm for the compliant occupant model and Sec. 5.1.2 covers the compliant occupant model impacting on its own without the landing gear.

5.1.1 Fixed Load Versus Variable Load

When the compliant occupant model was first introduced to the simulations, the damper was controlled to output the same fixed load as it was doing for the rigid

occupant model. Due to the complexities of the compliant occupant model and the interactions between the seat pan and the pelvis, this yielded very poor results, seen in Fig. 5.1.

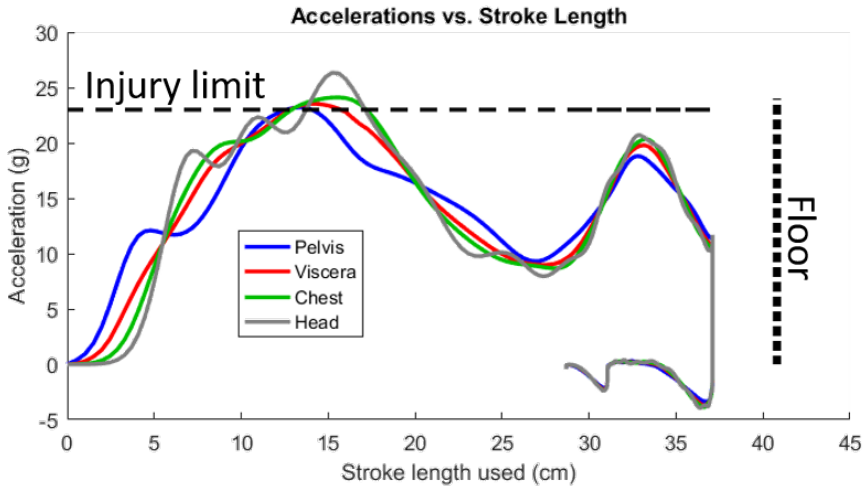

Figure 5.1: 50th percentile male accelerations from fixed load at 10.7 m/s

Even though this occupant is only impacting at 10.7 m/s, he quickly exceeds the 23g injury threshold. He is also stopped too early, therefore wasting stroke length, and then rebounds 8.4 cm. This is very undesirable and is directly caused by treating the compliant occupant model the same as the rigid occupant model. To rectify this, a variable load was used instead, seen in Fig. 5.2. This new control algorithm, described earlier in Eq. 3.4, adjusts as necessary to deal with the pelvis's effect on the seat pan. A constant force can be applied across the entire impact for the rigid occupant model because there are no interactions between the seat pan and the pelvis. However, in the compliant occupant model, the influence of the pelvis on the seat pan varies greatly throughout the impact.

Even though the force into the seat pan exceeds the injury threshold for the

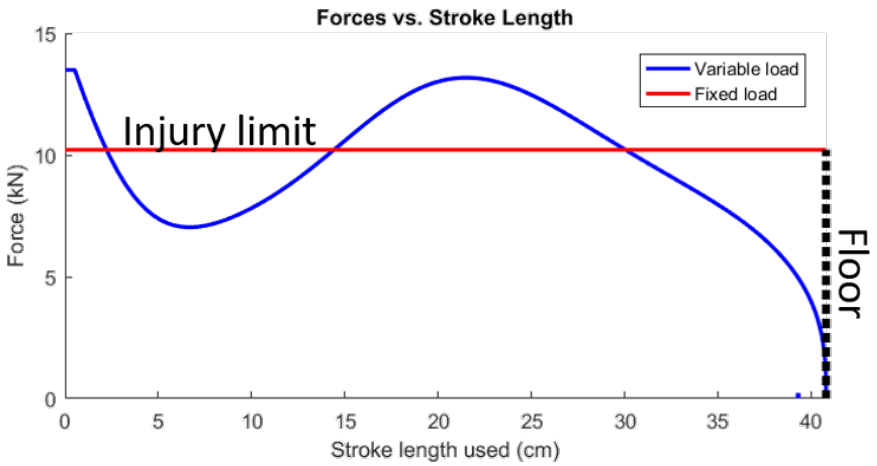

Figure 5.2: Fixed load and variable load

50th percentile male, this variable load interacts much better with the compliant occupant. The occupant's accelerations under this new loading can be seen in Fig. 5.3. Clearly, this variable loading provides a much smoother ride for the occupant and lowers the peak loads by $2.3g$ from $24.1g$ to $21.8g$. Additionally, this variable loading removes the secondary acceleration peak the occupant experienced with the fixed load and limits the rebound to 1.5 cm. The rebound is reduced even further at lower sink rates.

5.1.2 Compliant Occupant Model Results

With this new control algorithm, the compliant occupant model can be simulated and examined more closely. The 50th percentile male only reaches $21.8g$ when impacting at 10.7 m/s. Therefore, the first step in further analysis is increasing the speed until the $23g$ loading is met again. His sink rate can be increased to 11.2 m/s before exceeding the threshold because of the internal dynamics absorbing some

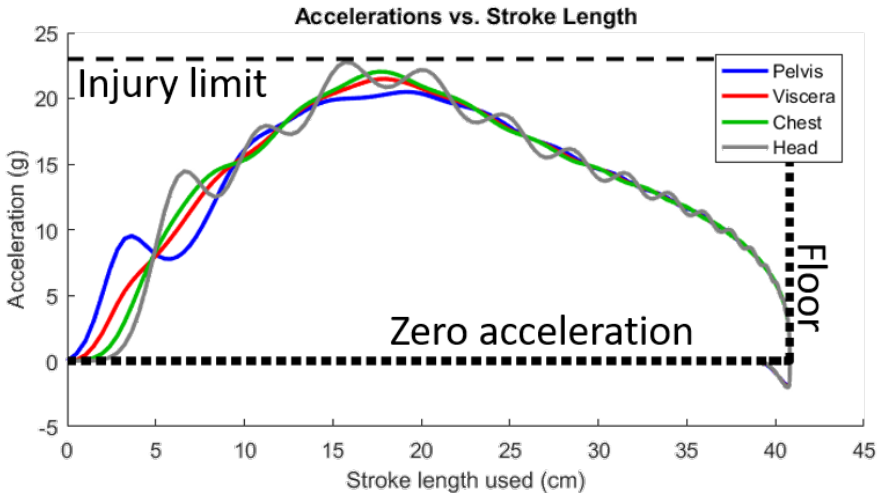

Figure 5.3: 50th percentile male accelerations at 10.7 m/s

of the energy. This new set of accelerations can be seen in Fig. 5.4.

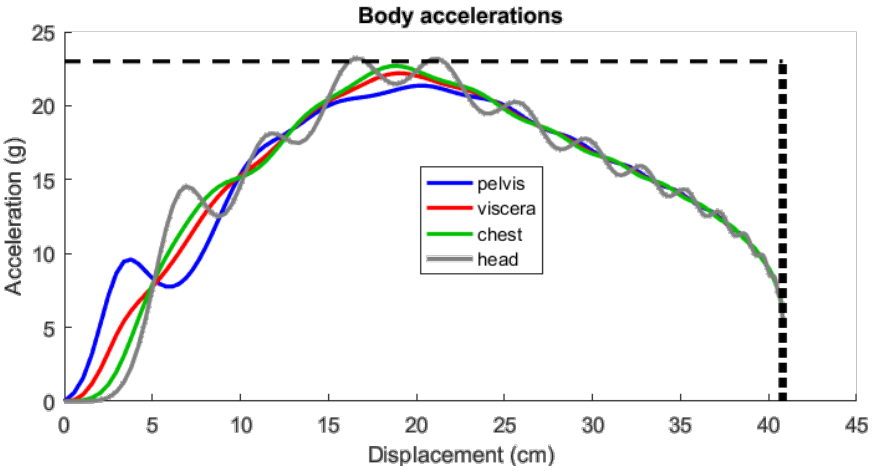

Figure 5.4: 50th percentile male accelerations at 11.2 m/s

However, the 5th percentile female does not fare so well at 11.2 m/s. Fig. 5.5 shows the chest accelerations, the component experiencing the highest accelerations, for each occupant at 11.2 m/s. The 5th percentile female clearly exceeds the injury threshold as she peaks at 25.2g. Her maximum safe sink rate must actually be reduced to 10.6 m/s so as not to pass her injury threshold. Meanwhile, the 95th

male does not exceed the injury threshold until 11.6 m/s. These values are tabulated in Table 5.1.

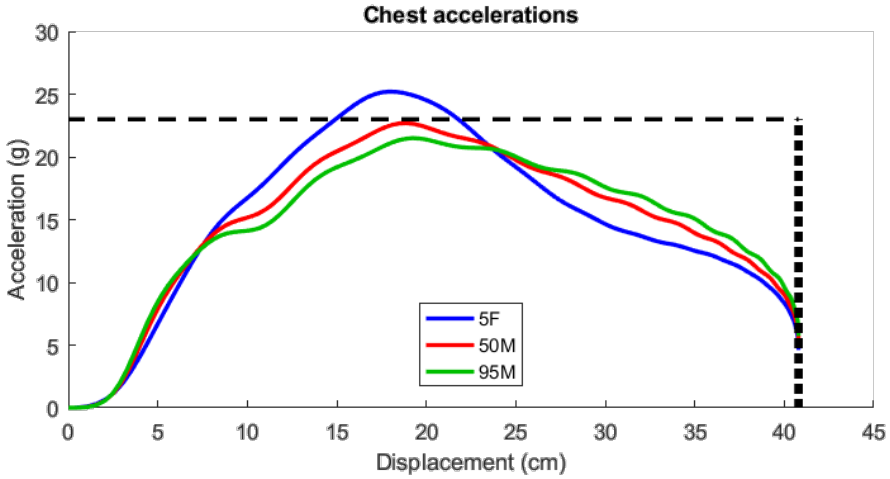

Figure 5.5: Occupant chest accelerations at 11.2 m/s

All three occupants have very similar load stroke profiles. Their accelerations from a 11.6 m/s impact with a constant stroking load landing gear are shown in Fig. 5.6.

5.2 Compliant Occupant Model and Landing Gear

With these new sink rate limits in mind, the landing gear model was added. The constant stroking load landing gear model was used in order to first determine the best-case scenario before including more realistic factors, such as a ramp up period for the force and the tapering off at the end, as seen in the hyperbolic tangent model and the sinusoidal model discussed in Sec. 2.3.

Fig. 5.7 shows the accelerations of the 50th percentile male at 11.2 m/s. The addition of the landing gear reduces the peak chest accelerations from by 1.8g

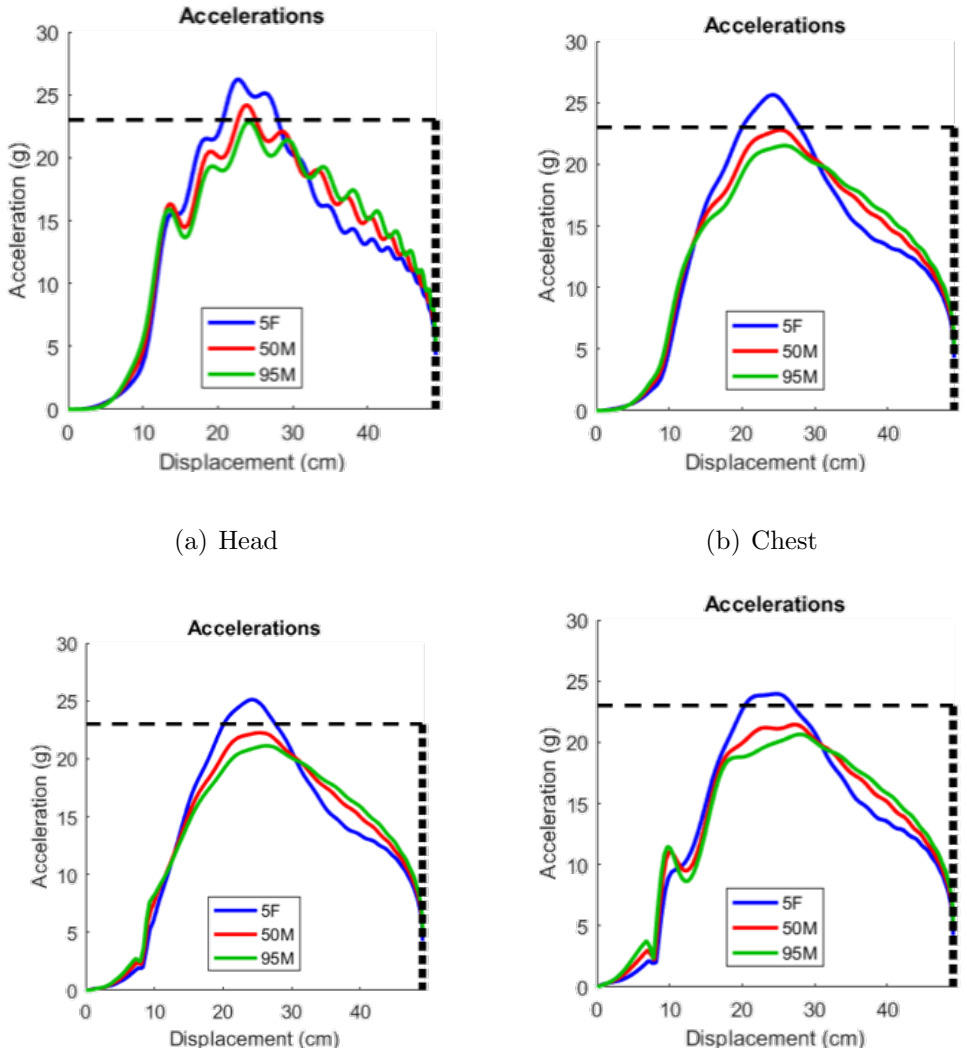

(a) Head

(b) Chest

(c) Viscera

(d) Pelvis

Figure 5.6: Compliant occupant component accelerations at 11.6 m/s with a constant stroking load landing gear

$23g$ to $21.2g$. This reduction in loading partially comes from the additional energy being absorbed by the occupant in the extra stroke length provided by the landing gear, which can be seen in the first 8 cm of the stroke. Since the occupant is no longer reaching the injury threshold, the sink rate can again be increased. The 50th percentile male can safely impact at 11.6 m/s when the most efficient landing gear is in place. However, the 5th percentile female again exceeds the $23g$ threshold at this sink rate, as seen in Fig. 5.8, and her maximum sink rate must be adjusted accordingly to 10.9 m/s. The 95th percentile male's maximum sink rate of 12.0 m/s is also tabulated in Table 5.1.

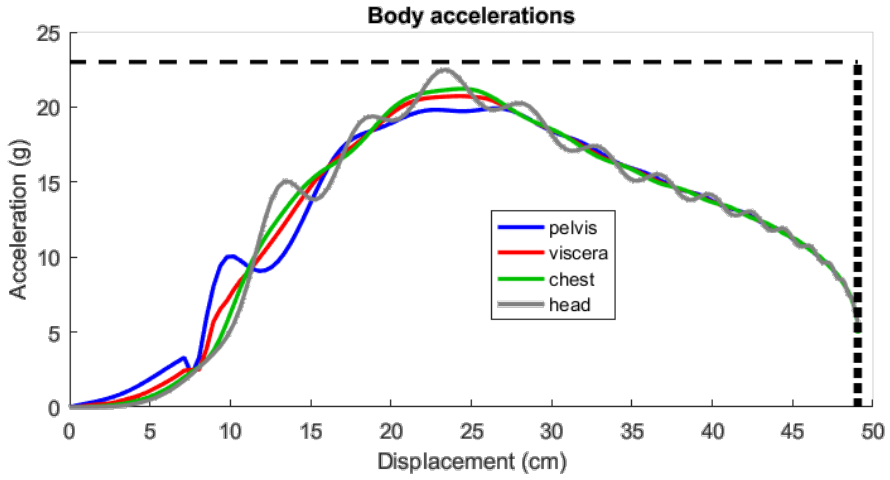

Figure 5.7: 50th percentile male accelerations at 11.2 m/s

Table 5.1: Maximum sink rate for each occupant

Occupant	Without landing gear	With sinusoidal landing gear	With constant stroking load landing gear
5^{th} percentile female	10.6 m/s	10.8 m/s	10.9 m/s
50^{th} percentile male	11.2 m/s	11.5 m/s	11.6 m/s
95^{th} percentile male	11.6 m/s	11.8 m/s	12.0 m/s

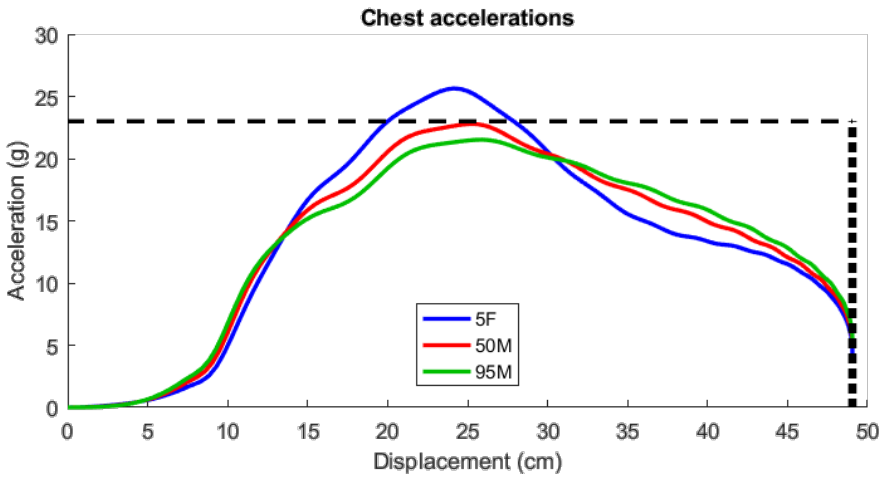

Figure 5.8: Each occupant's chest accelerations at 11.6 m/s

5.3 Complications

There are a number of issues that arise when adding in the landing gear system and when looking at the injury criteria for the compliant occupant model. Section 5.3.1 discusses the tradeoffs that must be made when trying to minimize destruction to the helicopter and Sec. 5.3.2 covers some of the issues that arise when trying to catalog the dangers to the compliant occupant.

5.3.1 Initial Forced Acceleration

While the landing gear clearly increases the maximum safe sink rate for each occupant, it also introduces a very stiff element to the system that has some detrimental effects to the occupant at low sink rates. The rigid occupant model's behavior with the landing gear system is described in Sec. 4.1. The negative effects seen in the ROM are amplified by the compliant occupant model. The landing gear

strokes at $6.7g$, shown in Fig. 4.4, and those loads are transmitted directly to the occupant because the seat is rigidly connected to the landing gear unless the landing gear has finished stroking or the loads to the occupant will exceed $14.5g$. While the rigid model showed that it also stroked at $6.7g$, the compliant occupant exhibits increased loads from those of the landing gear. These effects can most clearly be seen when comparing Fig. 5.9 and Fig. 5.10. In Fig. 5.9, the seat pan is allowed to stroke freely to absorb the energy from the 4 m/s impact. The loading peaks at $5g$ at the end, but the occupant does receive a safe, fairly smooth landing. Meanwhile, Fig. 5.10 shows the effects of the landing gear on the compliant occupant. The compliant occupant model shows that the occupant is launched at nearly $12g$ due to the landing gear, even though the sink rate is relatively low. This effect continues up to 6.5 m/s, where the occupant begins to see lower peak loads with the landing gear than without it.

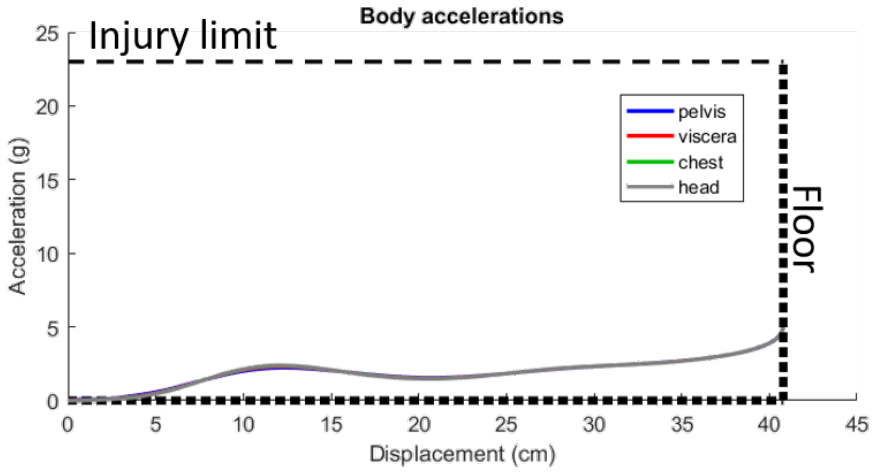

Figure 5.9: Behavior of compliant occupant model without landing gear at 4 m/s

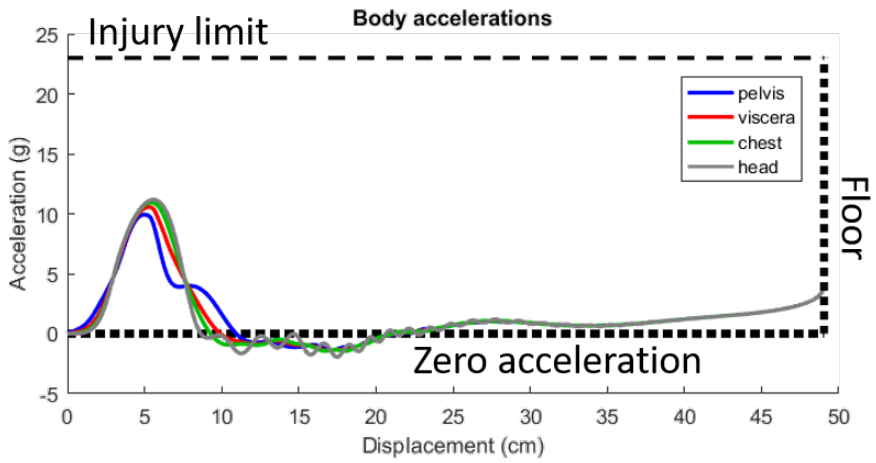

Figure 5.10: Behavior of compliant occupant model with landing gear at 4 m/s

5.3.2 Injury Criteria

Another issue faced in this research is determining which injury criteria to use in each crash case. As discussed in Sec. 1.3, most of the injury criteria developed previously were for the rigid occupant model. The compliant occupant model was not developed until 2015, and as such does not have as much documentation surrounding it. While the 14.5g acceleration threshold can easily be applied to the rigid occupant model, even transforming that acceleration into forces can lead to confusion. The rigid occupant model includes the seat pan mass, but when looking at the lumbar loads, the seat pan mass should not necessarily be included. However, the seat pan is typically included when looking at total body forces.

Meanwhile, these issues are exacerbated by the compliant occupant model's number of components. Special care needs to be taken when deciding whether to exclude the seat pan from that threshold and when determining how much of the occupant to use when looking at the lumbar loads. Fig. 5.11 shows the 50th

percentile male's lumbar loads when impacting at the maximum safe sink rate of 11.6 m/s, as determined by the $23g$ threshold. Even using a conservative injury threshold by excluding the seat pan mass from the force, these loads only reach 4.1 kN of compression. By this metric, the maximum safe sink rate would be significantly higher than that shown by the $23g$ threshold. There is clearly more research that needs to be done in this area in order to better improve these criteria.

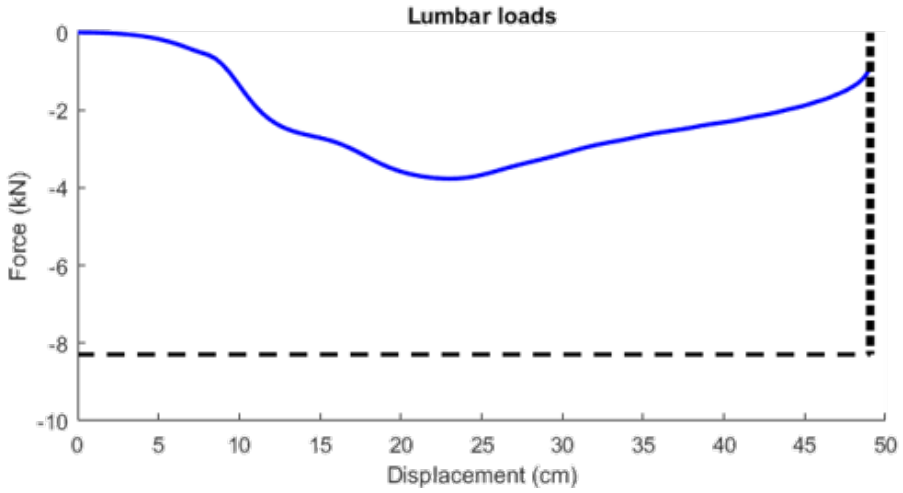

Figure 5.11: 50th percentile male's lumbar loads when impacting at 11.6 m/s

Chapter 6: Biodynamic Modeling

The purpose of this chapter is to detail the biodynamic modeling performed for Advanced Materials and Devices (AMAD). The University of Maryland was approached by AMAD as part of a Small Business Innovation Research (SBIR) project. The contract number was N0002417NR52468 and the primary person of contact was Barkan Kavlicoglu. AMAD was performing research into passive seat suspension systems and their effect on an occupant on a high-speed boat on rough waters. The University of Maryland was tasked with simulating a variety of stiffness and damping constants for the seat suspension and determining the occupant's peak loads under multiple acceleration impulses.

6.1 Introduction

To accomplish this task, the occupant model for the 95th percentile male were used. The masses, springs, and dampers are all the same values listed in Tables 2.2 and 2.3. However, AMAD wished to use a completely passive suspension system, so a spring was used in the seat instead of the MR damper that has been used previous simulations. The passive occupant models are shown below in Fig. 6.1. Some simulations also included a cushion between the seat pan and the pelvis,

whose models are shown in Fig. 6.1(b) and 6.1(d). The spring and damper constants from the cushion are handled in the model for this project in the same way they were included in Sec. 2.2.

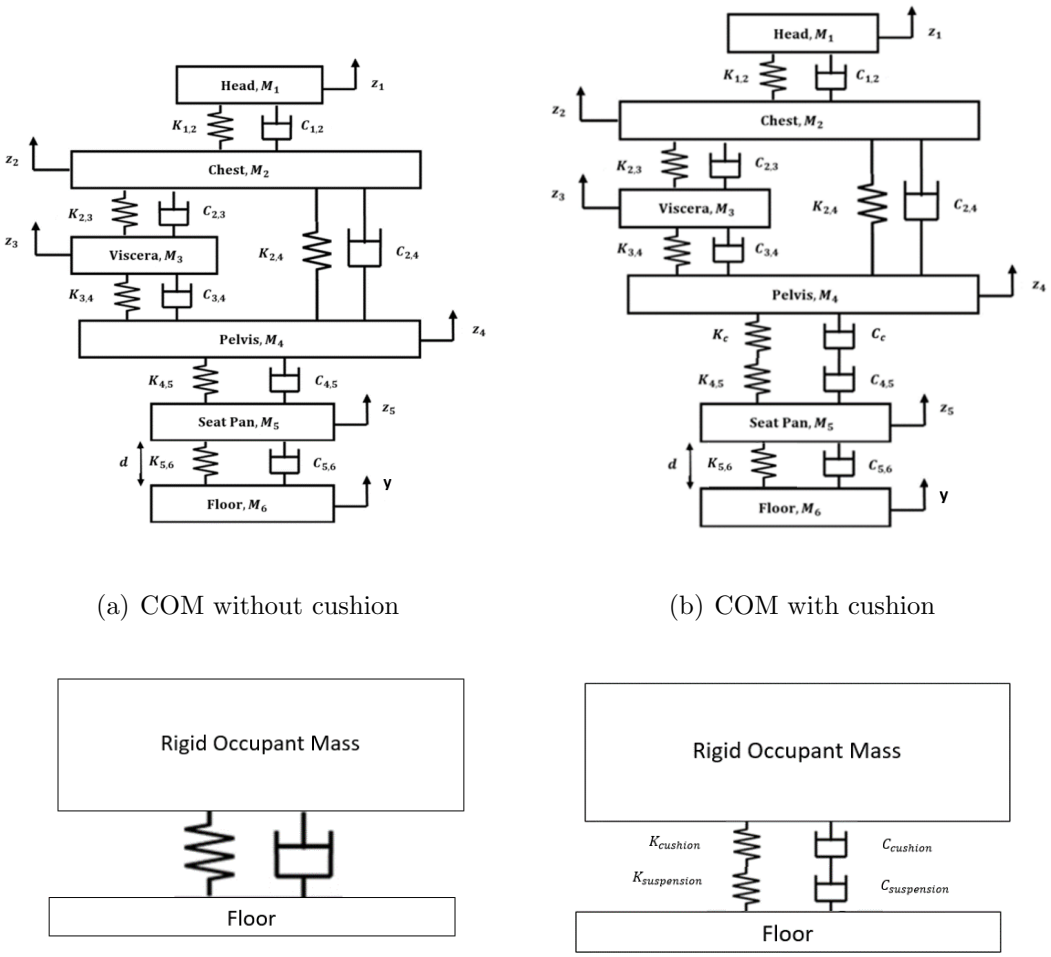

(a) COM without cushion

(b) COM with cushion

(c) ROM without cushion

(d) ROM with cushion

Figure 6.1: Occupant models

Through this research, the University of Maryland hoped to determine the effectiveness of AMAD's new devices to limit loads to the occupant in order to reduce discomfort or injury from extended, rough rides.

6.1.1 Ride Severity Index

Several injury criteria were considered when exploring the accelerations. In addition to the US Army Occupant Protection Handbook [33], which places a threshold at $23g$ at 7 ms, the Ride Severity Index (RSI) was investigated.

RSI is a new method of comparing the roughness of two acceleration pulses [34]. It uses a statistical approach to average the top 10% of the acceleration peaks and correlates that value to a level of discomfort over a specified time. This method is shown below in Eq. 6.1.

$$A_{1/10} = \frac{1}{n/10} \sum_{i=1}^{n/10} A_i \tag{6.1}$$

This $A_{1/10}$ value can then be compared to Table 6.1 to determine the occupant's condition over time. These resulting values can also be compared between rides to gauge how much rougher one ride was than another. For example, if Ride B has an $A_{1/10}$ value of $1.5g$ and Ride C has an $A_{1/10}$ value of $1.2g$, then the ratio between them is 1.25. Therefore, Ride B was 25% rougher, or more intense, than Ride C.

Table 6.1: Acceleration Severity Level [34]

Severity level	$A_{1/10}$ g	$A_{1/10}$ Range g	Occupant condition
IV	3	3-4	Extreme discomfort
III	NA	2-3	Discomfort and limited performance
II	1.5	1-2	Effective performance for 1-2 hours
I	1	<1	Effective performance for 4 or more hours

6.2 Results

The results for both halves of this project are discussed below in Sec. 6.2.1 and 6.2.2. Section 6.2.1 discusses the initial nine cases that were requested. These cases did not include a seat cushion. Sec. 6.2.2 involved a much wider range of parameters, including both occupant models, and with and without a seat cushion.

6.2.1 Initial Nine Cases

Several floor input requirements were given for the simulations. Initially, a single, $5g$, 200 ms triangular peak was requested and many of the simulations were performed based on this requirement. Later, a sinusoidal input was requested, so the simulations were changed to reflect that. Since waves occur repeatedly, the requirement was changed to three sequential peaks, and eventually a long series of peaks from a test on a boat were provided for the simulations. Each of these inputs can be seen in Fig. 6.2.

Initially, nine different cases were desired. AMAD provided UMD with three stiffnesses of 100, 125, and 150 lbf/in (17.5, 21.9, and 26.3 kN/m) and three damping constants of 33.3, 41.7, and 50 $lbf.s/in$ (5831, 7302, and 8756 Ns/m). These first nine cases were simulated using the single, $5g$ triangular peak. Their peak loads, mechanical attenuation, and biodynamic attenuation are all shown in Table 6.2.

The results from Table 6.2 are also shown in Fig. 6.3. Clearly, the seat pan suspension parameters are spread over too narrow of a range to have a large effect

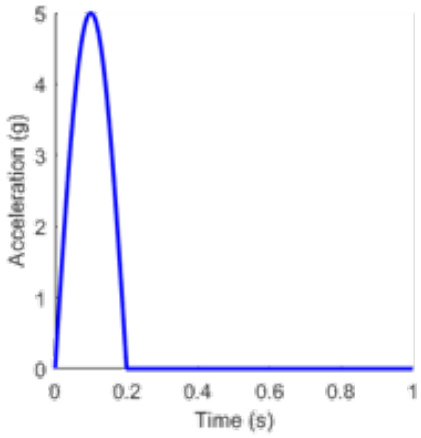

(a) Sinusoidal wave

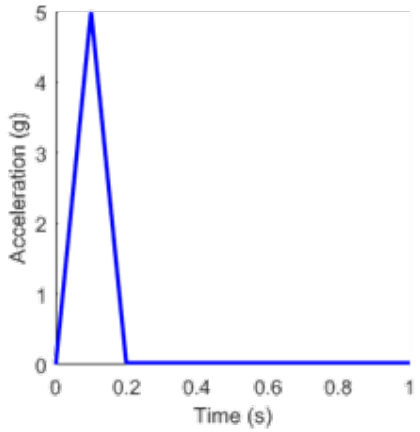

(b) Single triangular peak

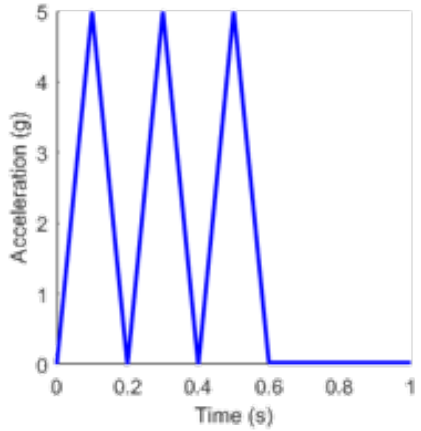

(c) Three triangular peaks

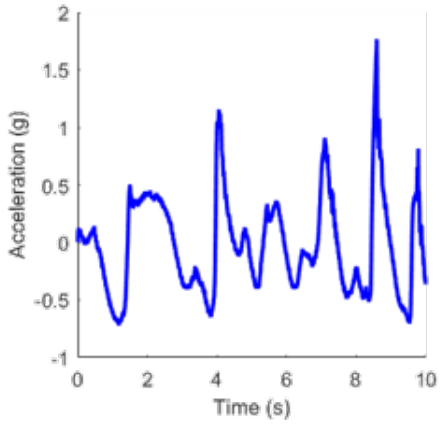

(d) Long series of peaks

Figure 6.2: Acceleration inputs

Table 6.2: Biodynamic Modeling Simulation Results

Spring Constant kN/m	Damping Constant Ns/m	Natural Frequency Hz	Damping Ratio	Peak Seat Pan Acceleration g	Mechanical Attenuation g	Peak Biodynamic Acceleration	Biodynamic Attenuation g
17.512	5831	2.20	2.31	3.817	.763	6.268	1.254
17.512	7302	2.20	2.89	3.877	.775	6.420	1.284
17.512	8756	2.20	3.46	3.903	.781	6.531	1.306
21.890	5831	2.47	2.06	3.832	.766	6.311	1.262
21.890	7302	2.47	2.58	3.884	.777	6.450	1.290
21.890	8756	2.47	3.10	3.904	.781	6.554	1.311
26.268	5831	2.70	1.88	3.845	.769	6.353	1.271
26.268	7302	2.70	2.36	3.891	.778	6.480	1.296
26.268	8756	2.70	2.83	3.907	.781	6.576	1.315

on the occupant's accelerations. In general though, as the stiffness and damping increases, so do the accelerations. Additionally, while the pelvis is the only component of the body being shown in Fig. 6.3, all of the body accelerations are almost identical at these low g loads. This fact is also shown in Fig. 6.4, which shows all of the accelerations in a single run. In an impact at these lower loads, the occupant itself is almost completely rigid and nearly all of the motion stems from the seat pan and pelvic interactions.

6.2.2 Additional Cases

The second half of this project contained a much wider range of parameters. The spring values considered were 50, 100, and 150 lbf/in and the damper values were 50, 100, and 150 $lbf.s/ft$. Additionally, a seat cushion was included in some of the models. Its spring values were 15, 22.5, and 30 lbf/in and its damper values were 25, 50, and 100 $lbf.s/ft$. Finally, a long set of acceleration pulses from a

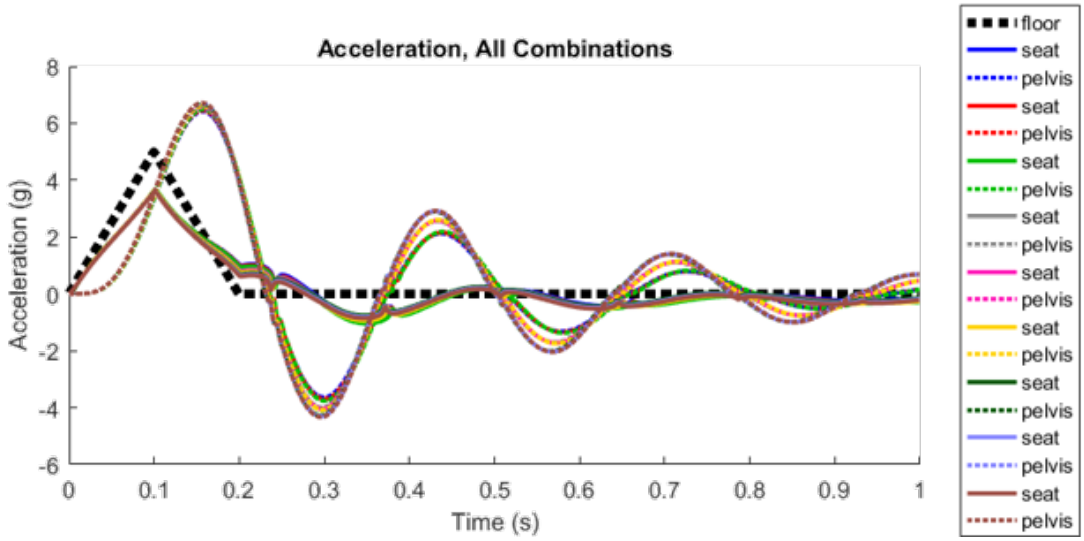

Figure 6.3: Seat and pelvic accelerations for all nine cases

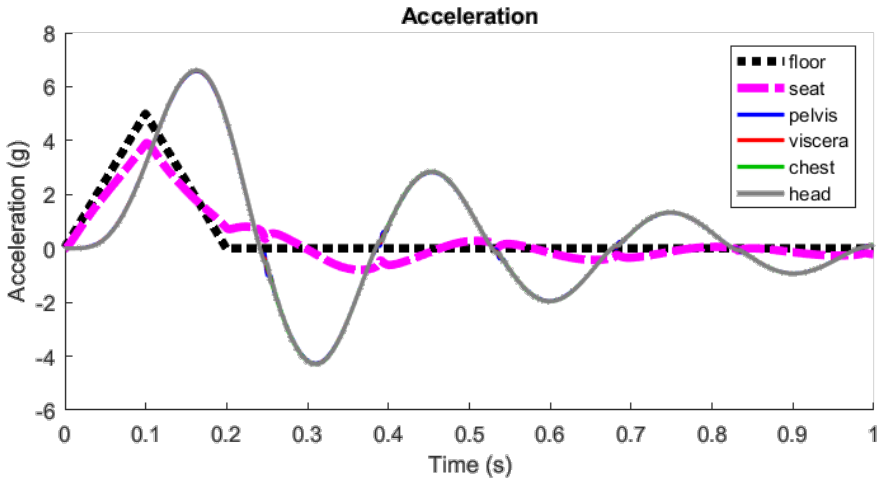

Figure 6.4: Accelerations for single occupant

boat test was provided for these simulations, which had an $A_{1/10}$ value of $2.98g$. Combinations of these parameters were combined and the 95th percentile male's acceleration responses were recorded from each simulation. The $A_{1/10}$ values from the seat pan and pelvis were then compared to that of the wave input to determine if the combination of parameters increased or decreased the loads to the occupant.

The simulations included multiple runs for each occupant model, with and without a cushion, each with a different array of seat parameters. Table 6.3 highlights the minimum and maximum loads from each of these different combinations.

Table 6.3: Acceleration Loads and System Parameters

Max/Min loads	Seat pan acceleration $[g]$	Pelvis acceleration $[g]$	K_s	C_s	K_c	C_c	Occupant model
Max	3.80	-	150	50	-	-	Rigid
Min	2.58	-	50	100	-	-	Rigid
Max	2.60	-	50	100	30	25	Rigid
Min	1.68	-	50	100	15	100	Rigid
Max	4.67	4.12	150	50	-	-	Compliant
Min	3.05	3.05	50	100	-	-	Compliant
Max	2.24	2.77	50	100	30	25	Compliant
Max	2.40	2.45	109.5	132	22.5	100	Compliant
Min	2.00	2.06	50	100	15	100	Compliant

The floor acceleration pulse provided for this series of cases was nearly ten minutes long. For these simulations, only the first two minutes were used in an effort to save on computing time. A typical case is shown below in Fig. 6.5. Additionally, the frequency responses are shown in Fig. 6.6. These plots help to show the frequencies at which the occupant will show the greatest response.

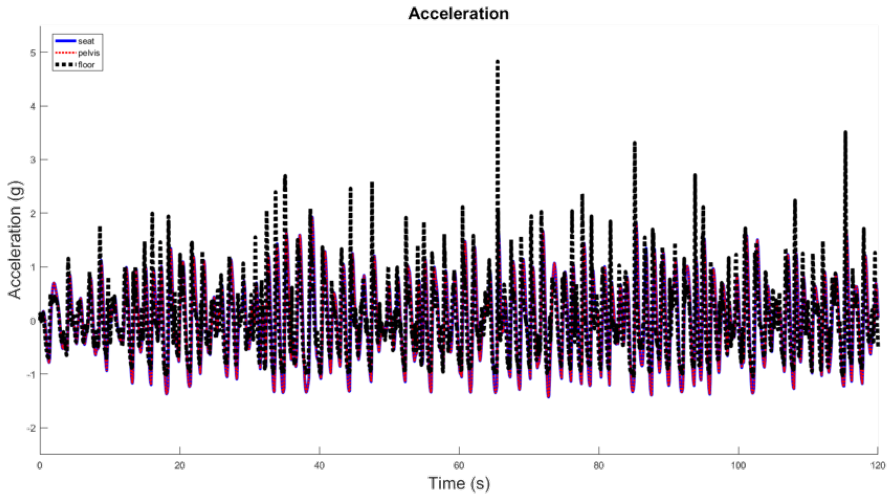

Figure 6.5: Typical accelerations for a single case

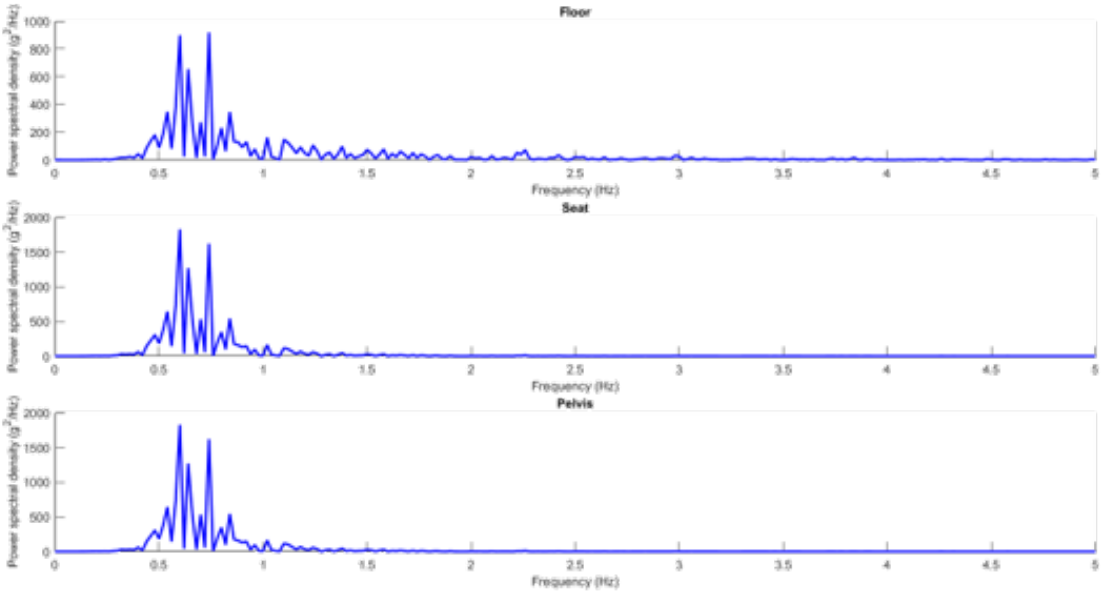

Figure 6.6: Typical frequency response for a single case

Chapter 7: Conclusion

The purpose of this chapter is to summarize the research that has been done on this project and to discuss areas of future work. Additionally, the long term schedule of this project is described.

The goal of this research was to develop a comprehensive model of an occupant in a helicopter equipped with an active seat and an active landing gear system to simulate crash landings and determine the effectiveness of various energy absorbing devices. This research began with designing a seat control algorithm for the rigid occupant model alone. Then the compliant occupant model was substituted in and adjustments were made to the control algorithm to accommodate the additional motion of the COM. Eventually, the landing gear model was added to the system and its effect on the rigid occupant's loads was examined. Later, the landing gear was applied to the compliant occupant model. The load-stroke profiles for each landing gear and occupant were determined and the maximum safe sink rate with each device was found.

7.1 Rigid Occupant Model

The rigid occupant model was initially used as a simple solution to estimate the loads transmitted to the occupant in the event of a helicopter crash. A viscous damper was originally used to absorb the energy and it was determined that a 50th percentile male could impact at 7.25 m/s without exceeding his injury threshold of $14.5g$ using this system. The viscous system is very inefficient, so a fixed load energy absorber was examined. This device is much more efficient and raised the maximum safe sink rate for the 50th percentile male to 10.7 m/s. However, the FLEA is also a passive device that cannot adapt to different occupants or sink rates. This causes the 5th percentile female to always exceed her injury threshold and is inefficient on the 95th percentile male.

An MR damper was added to the seat pan in order to work with the viscous damper and adapt to the variable impact conditions. This device was controlled to produce a net force that caused the peak loads to drop by 50% when compared to the purely viscous system. This new system was then applied to all three occupants. The controllable load allowed the entire range of occupants to experience a soft landing and use the entire stroke length up to 10.7 m/s.

Finally, the landing gear model was added to the seat and occupant models. The constant stroking landing gear was initially used to determine the best case scenario for the occupant. This landing gear model increased the maximum safe sink rate for all three occupants to 11.2 m/s. The more realistic, sinusoidal landing gear increases the maximum sink rate from 10.7 m/s to 11.1 m/s. These simulations

informed the control algorithms for the compliant occupant model.

7.2 Compliant Occupant Model

The compliant occupant model was introduced after the rigid occupant model's control algorithm was developed. This model was used to give more insight into the loads within the occupant and understand the interactions between the seat pan and the occupant. Unlike the rigid occupant model, which shows the occupants following the same load stroke profile across all the occupants, the compliant model exhibits slightly different behaviors depending on which occupant mass is simulated. This led to the maximum safe sink rate for the 50th percentile male reaching 11.2 m/s, but the 5th percentile female only reaching 10.6 m/s and the 95th percentile male achieving 11.6 m/s.

These maximums were increased when the landing gear model was implemented with the compliant occupant models. The sinusoidal landing gear increased each occupant's maximum safe sink rate by 0.2-0.3 m/s each, and the more efficient constant stroking load landing gear increased each maximum safe sink rate by an additional 0.1-0.2 m/s on top of that. All of these values are tabulated in Table 7.1.

Both occupant models experience detrimental effects from the landing gear at low sink rates, but these effects are particularly prevalent in the compliant occupant model. The landing gear strokes at $6.7g$, which propagates through to the compliant occupant and forces it to experience nearly $12g$. This effect eventually is offset by the landing gear's energy absorption capabilities at sink rates above 7.9

Table 7.1: Maximum Sink Rate for Each Occupant

Occupant	Without landing gear	With sinusoidal landing gear	With constant stroking load landing gear
All rigid occupants	10.7 m/s	11.1 m/s	11.2 m/s
5^{th} percentile Female	10.6 m/s	10.8 m/s	10.9 m/s
50^{th} percentile Male	11.2 m/s	11.5 m/s	11.6 m/s
95^{th} percentile Male	11.6 m/s	11.8 m/s	12.0 m/s

m/s. The compliant occupant's loads are always well below the injury criteria, but these loads could still cause mild injury and are a trade off when designing a system to protect the helicopter.

7.3 Future Work

As stated in chapter 5, a heavier occupant can withstand higher sink rates. None of the masses used in these simulations contain a complete set of limbs or any additional equipment that would typically be seen in a military pilot. There could be some interesting results in determining what the average pilot carries with him or her on a typical flight and how those additional masses affect the accelerations and the maximum sink rate.

Additionally, further research needs to be performed to determine the injury criteria for the compliant occupant model. Sections 1.3 and 5.3.2 discuss the background and some of the issues with the current injury criteria and how they apply to the compliant model. These conditions need to be resolved as the $14.5g$ threshold on the rigid occupant and the $23g$ threshold on the compliant model's

chest are currently the limiting factors on the maximum safe sink rate. A threshold for the lumbar load compression should be researched so that these loads can be used to their fullest potential.

There has also been some research done into the presence of a seat cushion and its effects on the occupant. Typically, a seat cushion model was adding oscillations and was eventually neglected for simplicity. However, seat cushions are common devices due to the comfort they add to a more typical ride and they should be investigated to determine if there is a good combination of stiffness and damping that can provide a comfortable ride that is also safe in the case of an impact.

Finally, the floor is the last primary location for energy absorption in a helicopter. So far, this research has considered the floor to have a rigid connection with the landing gear, but that is not the case in a real crash. The floor collapses in a controlled manner just like the landing gear and seat pan. This energy absorption is not yet modeled in these simulations and giving it a honeycomb-like crushing profile is a good place to start to better understand how the floor works with the landing gear and seat.

7.3.1 VLRCOE

This research is part of a series of projects funded by the US Army, Navy, and NASA in the Vertical Lift Rotorcraft Centers of Excellence (VLRCOE) project. This research specifically is Task 1.15 at the University of Maryland and is finishing its second year in a five year project. As such, this project has specific tasks to be

accomplished in the next three years, and these tasks are listed below:

- Year 3
  - Develop models of energy absorbers based on pneumatic and shape memory alloy elements
  - Test these energy absorbing prototypes at low speeds ($< 10\ ft/s$) on the drop tower in the lab at UMD
- Year 4
  - Validate the energy absorber models and feedback control strategies with experimental test data from the UMD drop tower for high speeds ($> 10\ ft/s$)
  - Refine crashworthiness simulations to incorporate models of adaptive energy absorbers
  - Assess capabilities of new energy absorber designs to minimize injury criteria
  - Refine controllers
- Year 5
  - Quantify injury mitigation probabilities using simulations
  - Assess biodynamic crew response and refine controllers and energy absorber designs

Additionally, during the annual review in November, some other recommendations were made. The sponsors would like to see the MR damper results be directly compare to other systems already being used in the field or under development to better determine how benefits of MR. Some interest was also shown in adding a seat cushion, which has previously been ignored because of its added oscillations that could not be resolved. Overall, though, the sponsors were pleased with how the project has gone in its first two years and are looking forward to the experimental results from the drop tests in the coming years.

Bibliography

[1] Karen E Jackson. Advances in rotorcraft crashworthiness: Trends leading to improved survivability 37th alexander a. nikolsky honorary lecture. *Journal of the American Helicopter Society*, 63(2):1–25, 2018.

[2] Stanley P Desjardins and Harold D Harrison. The design, fabrication, and testing of an integrally armored crashworthy crew seat. Technical report, DYNAMIC SCIENCE ENGINEERING OPERATIONS PHOENIX AZ, 1972.

[3] A Martin Eiband. Human tolerance to rapidly applied accelerations: a summary of the literature. 1959.

[4] Louise A Ahure-Powell. *Magnetorheological fluids and applications to adaptive landing gear for a lightweight helicopter*. PhD thesis, University of Maryland, College Park, 2014.

[5] Justin Littell. Full-scale crash test of an md-500 helicopter. 2011.

[6] Young-Tai Choi, Ryan Robinson, Wei Hu, Norman M Wereley, Terrence S Birchette, Akif O Bolukbasi, and Jin Woodhouse. Analysis and control of a magnetorheological landing gear system for a helicopter. *Journal of the American Helicopter Society*, 61(3):1–8, 2016.

[7] Louise A Ahuré Powell, Young T Choi, Wei Hu, and Norman M Wereley. Nonlinear modeling of adaptive magnetorheological landing gear dampers under impact conditions. *Smart Materials and Structures*, 25(11):115011, 2016.

[8] Richard E Zimmerman, James C Warrick, Alan D Lane, Norman A Merritt, and Akif O Bolukbasi. Aircraft crash survival design guide. volume 3. aircraft structural crash resistance. Technical report, SIMULA INC PHOENIX AZ, 1989.

[9] Dennis F Shanahan. Basic principles of helicopter crashworthiness. Technical report, ARMY AEROMEDICAL RESEARCH LAB FORT RUCKER AL, 1993.

[10] Military Standard. Mil-std-1290,. *Light Fixed and Rotary-Wing Aircraft Resistance, Department of Defense, United States of America*, 1995.

[11] C Hudson Carper, LeRoy T Burrows, and Kent F Smith. Army helicopter crashworthiness. Technical report, ARMY RESEARCH AND TECHNOLOGY LABS FORT EUSTIS VA APPLIED TECHNOLOGY LAB, 1983.

[12] John W Melvin, Kenneth J Baron, William C Little, Thomas W Gideon, and John Pierce. Biomechanical analysis of indy race car crashes. Technical report, SAE Technical Paper, 1998.

[13] K Vasantha Kumar and William T Norfleet. Issues on human acceleration tolerance after long-duration space flights. 1992.

[14] Ravi Thyagarajan, Jaisankar Ramalingam, and Kumar B Kulkarni. Comparing the use of dynamic response index (dri) and lumbar load as relevant spinal injury metrics. Technical report, ARMY TANK AUTOMOTIVE RESEARCH DEVELOPMENT AND ENGINEERING CENTER WARREN MI, 2014.

[15] NATO STANAG. 4569. *Protection Levels for Occupants of logistic and Light Armored Vehicles*, 2004.

[16] National Highway Traffic Safety Administration et al. 571.208 standard no. 208; occupant crash protection. *Federal Motor Vehicle Safety Standards and Regulations*, 2004.

[17] Young-Tai Choi and Norman M Wereley. Biodynamic response mitigation to shock loads using magnetorheological helicopter crew seat suspensions. *Journal of Aircraft*, 42(5):1288–1295, 2005.

[18] Chaoyang Guo, Xinglong Gong, Shouhu Xuan, Luhang Zong, and Chao Peng. Normal forces of magnetorheological fluids under oscillatory shear. *Journal of Magnetism and Magnetic Materials*, 324(6):1218–1224, 2012.

[19] Gregory J Hiemenz, Young-Tai Choi, and Norman M Wereley. Semi-active control of vertical stroking helicopter crew seat for enhanced crashworthiness. *Journal of aircraft*, 44(3):1031–1034, 2007.

[20] L Wei and MJ Griffin. Mathematical models for the apparent mass of the seated human body exposed to vertical vibration. *Journal of Sound and Vibration*, 212(5):855–874, 1998.

[21] XX Liu, J Shi, GH Li, X Le, B Zhao, M Yue, J Liu, G Bai, and W Ke. Biodynamic response and injury estimation of ship personnel to ship shock motion induced by underwater explosion. In *Proceeding of 69th Shock and Vibration Symposium*, volume 18, pages 1–18, 1998.

[22] W Qassem and MO Othman. Vibration effects on setting pregnant womensubjects of various masses. *Journal of biomechanics*, 29(4):493–501, 1996.

[23] Harinder J Singh and Norman M Wereley. Biodynamic model of a seated occupant exposed to intense impacts. *AIAA Journal*, 53(2):426–435, 2014.

[24] Karen E Jackson, Edwin L Fasanella, Richard Boitnott, Joseph McEntire, and Alan Lewis. Occupant responses in a full-scale crash test of the sikorsky acap helicopter. *Journal of the American Helicopter Society*, 49(2):127–139, 2004.

[25] Humanetics Innovative Solutions. Hybrid ii 50th male dummy. *Frontal Impact Crash Test Dummies, URL: http://www. humaneticsatd. com/crash-test-dummies/frontalimpact/hybrid-ii-50th [cited March 31, 2016]*, 2017.

[26] JW Coltman, CV Ingen, NB Johnson, and RE Zimmerman. Aircraft crash survival design guide. volume 2. aircraft design crash impact conditions and human tolerance. Technical report, SIMULA INC PHOENIX AZ, 1989.

[27] Justin D Littell, Karen E Jackson, and Sotiris Kellas. Crash test of an md-500 helicopter with a deployable energy absorber concept. 2010.

[28] Stanley P Desjardins. The evolution of energy absorption systems for crashworthy helicopter seats. *Journal of the American Helicopter Society*, 51(2):150–163, 2006.

[29] Harinder J Singh and Norman M Wereley. Model-based optimal control of biodynamic response to vertical crash loads for an occupant seated in a helicopter. In *AHS 69 th Annual Forum*, 2013.

[30] Harinder Singh and Norman Wereley. Influence of occupant compliance on optimal control performance of a vertically stroking seat suspension. In *53rd AIAA/ASME/ASCE/AHS/ASC Structures, Structural Dynamics and Materials Conference 20th AIAA/ASME/AHS Adaptive Structures Conference 14th AIAA*, page 1879, 2012.

[31] Harinder J Singh, Young-Tai Choi, and Norman M Wereley. Optimal control of vertically stroking crew seats employing magnetorheological energy absorbers. In *ASME 2009 Conference on Smart Materials, Adaptive Structures and Intelligent Systems*, pages 539–550. American Society of Mechanical Engineers, 2009.

[32] HJ Singh, YT Choi, and NM Wereley. Optimal terminal trajectory control of vertically stroking crew seats using magnetorheological energy absorbers. In *Proceedings of 51st AIAA/ASME/ASCE/AHS/ASC Structures, Structural Dynamics and Materials Conference*, pages 12–15.

[33] US Army Occupant Crash Protection Handbook. for tactical ground vehicles, 2000.

[34] Michael R Riley, Tim Coats, Kelly Haupt, and Donald Jacobson. Ride severity index: A simplified approach for comparing peak acceleration responses of high-speed craft. *Journal of Ship Production and Design*, 29(1):25–35, 2013.